



OPEN ACCESS

EDITED BY

Thorvaldur Thordarson,
University of Iceland, Iceland

REVIEWED BY

Karoly Nemeth,
Massey University, New Zealand
Bruce Houghton,
University of Hawaii, United States

*CORRESPONDENCE

S. Calvari,
sonia.calvari@ingv.it

SPECIALTY SECTION

This article was submitted to
Volcanology,
a section of the journal
Frontiers in Earth Science

RECEIVED 18 March 2022

ACCEPTED 04 July 2022

PUBLISHED 22 August 2022

CITATION

Calvari S, Di Traglia F, Ganci G, Bruno V, Ciancitto F, Di Lieto B, Gambino S, Garcia A, Giudicepietro F, Inguaggiato S, Vita F, Cangemi M, Inguaggiato C, Macedonio G, Mattia M, Miraglia L, Nolesini T, Pompilio M, Romano P, Salerno G, Casagli N, Re G, Del Carlo P, Di Roberto A, Cappello A, Corradino C, Amato E, Torrisi F, Del Negro C, Esposito AM, De Cesare W, Caputo T, Buongiorno MF, Musacchio M, Romaniello V, Silvestri M, Marotta E, Avino R, Avvisati G and Belviso P (2022), Multi-parametric study of an eruptive phase comprising unrest, major explosions, crater failure, pyroclastic density currents and lava flows: Stromboli volcano, 1 December 2020–30 June 2021. *Front. Earth Sci.* 10:899635. doi: 10.3389/feart.2022.899635

COPYRIGHT

© 2022 Calvari, Di Traglia, Ganci, Bruno, Ciancitto, Di Lieto, Gambino, Garcia, Giudicepietro, Inguaggiato, Vita, Cangemi, Inguaggiato, Macedonio, Mattia, Miraglia, Nolesini, Pompilio, Romano, Salerno, Casagli, Re, Del Carlo, Di Roberto, Cappello, Corradino, Amato, Torrisi, Del Negro, Esposito, De Cesare, Caputo, Buongiorno, Musacchio, Romaniello, Silvestri, Marotta, Avino, Avvisati and Belviso. This is an open-access article distributed under the terms of the [Creative Commons Attribution License \(CC BY\)](https://creativecommons.org/licenses/by/4.0/). The use, distribution or reproduction in other forums is permitted, provided the

Multi-parametric study of an eruptive phase comprising unrest, major explosions, crater failure, pyroclastic density currents and lava flows: Stromboli volcano, 1 December 2020–30 June 2021

S. Calvari^{1*}, F. Di Traglia², G. Ganci¹, V. Bruno¹, F. Ciancitto¹, B. Di Lieto³, S. Gambino¹, A. Garcia⁴, F. Giudicepietro³, S. Inguaggiato⁵, F. Vita⁵, M. Cangemi⁶, C. Inguaggiato^{4,7}, G. Macedonio³, M. Mattia¹, L. Miraglia¹, T. Nolesini⁸, M. Pompilio⁹, P. Romano³, G. Salerno¹, N. Casagli^{2,10}, G. Re⁹, P. Del Carlo⁹, A. Di Roberto⁹, A. Cappello¹, C. Corradino¹, E. Amato^{1,11}, F. Torrisi^{1,12}, C. Del Negro¹, A. M. Esposito³, W. De Cesare³, T. Caputo³, M. F. Buongiorno¹³, M. Musacchio¹³, V. Romaniello¹³, M. Silvestri¹³, E. Marotta³, R. Avino³, G. Avvisati³ and P. Belviso³

¹Istituto Nazionale di Geofisica e Vulcanologia, Osservatorio Etneo—Sezione di Catania, Catania, Italy, ²National Institute of Oceanography and Applied Geophysics—OGS, Sgonico, Italy, ³Istituto Nazionale di Geofisica e Vulcanologia, Osservatorio Vesuviano, Napoli, Italy, ⁴Istituto Nazionale di Geofisica e Vulcanologia, Sezione di Bologna, Bologna, Italy, ⁵Istituto Nazionale di Geofisica e Vulcanologia, Sezione di Palermo, Palermo, Italy, ⁶DiSTeM, Università degli Studi di Palermo, Palermo, Italy, ⁷Departamento de Geología, Centro de Investigación Científica y de Educación Superior de Ensenada, Baja California (CICESE), Ensenada, Mexico, ⁸Università degli Studi di Firenze—Centro per la Protezione Civile, Firenze, Italy, ⁹Istituto Nazionale di Geofisica e Vulcanologia, Sezione di Pisa, Pisa, Italy, ¹⁰Dipartimento di Scienze della Terra, Università degli Studi di Firenze, Firenze, Italy, ¹¹Department of Mathematics and Computer Science, University of Palermo, Palermo, Italy, ¹²Department of Electrical, Electronic and Computer Engineering, University of Catania, Catania, Italy, ¹³Istituto Nazionale di Geofisica e Vulcanologia, Osservatorio Nazionale Terremoti, Rome, Italy

Open conduit volcanoes like Stromboli can display elusive changes in activity before major eruptive events. Starting on December 2020, Stromboli volcano displayed an increasing eruptive activity, that on 19 May 2021 led to a crater-rim collapse, with pyroclastic density currents (PDCs) that spread along the barren NW flank, entered the sea and ran across it for more than 1 km. This episode was followed by lava flow output from the crater rim lasting a few hours, followed by another phase of lava flow in June 2021. These episodes are potentially very dangerous on island volcanoes since a landslide of hot material that turns into a pyroclastic density current and spreads on the sea surface can threaten mariners and coastal communities, as happened at Stromboli on 3 July and 28 August 2019. In addition, on entering the sea, if their volume is large enough,

landslides may trigger tsunamis, as occurred at Stromboli on 30 December 2002. In this paper, we present an integration of multidisciplinary monitoring data, including thermal and visible camera images, ground deformation data gathered from GNSS, tilt, strainmeter and GBInSAR, seismicity, SO₂ plume and CO₂ ground fluxes and thermal data from the ground and satellite imagery, together with petrological analyses of the erupted products compared with samples from previous similar events. We aim at characterizing the preparatory phase of the volcano that began on December 2020 and led to the May–June 2021 eruptive activity, distinguishing this small intrusion of magma from the much greater 2019 eruptive phase, which was fed by gas-rich magma responsible for the paroxysmal explosive and effusive phases of July–August 2019. These complex eruption scenarios have important implications for hazard assessment and the lessons learned at Stromboli volcano may prove useful for other open conduit active basaltic volcanoes.

KEYWORDS

Stromboli volcano, multi-disciplinary monitoring data, crater-rim collapse, pyroclastic density current, hazard assessment

1 Introduction

Open conduit volcanoes characterized by frequent eruptive activity often display very subtle changes forecasting major events. Stromboli volcano is one of these, and in this paper we focus on a recent eruptive phase that grew very slowly, displaying unrest, major explosions, lava flows and ultimately crater failure, analyzing these events from a multidisciplinary point of view in order to gather insights useful for hazard purposes. In addition, we seek to verify if it is possible to distinguish in advance from the monitoring signals any small batch of magma rising up along the feeding system from a much more voluminous supply like the one leading to the 2019 eruptive phase, which was fed by gas-rich low-porphyrific (LP) magma (Andronico et al., 2021; Giordano and De Astis, 2021).

Stromboli is the easternmost, most recent and most active volcano comprising the Aeolian Archipelago calc-alkaline volcanic arc in the southern Tyrrhenian Sea (Figure 1A). The volcano has a conical shape, with a ~4.5 km wide base of the emergent edifice (Figure 1B), and rises 924 m above sea level (a.s.l.), but extends below the sea surface down to ~2000 m depth (Romagnoli et al., 1993; Romagnoli and Casalbone, 2013). The volcano is slightly elongated in a NE-SW direction (Figure 1) following the main structural trend affecting the easternmost branch of the archipelago (Francalanci et al., 2013).

Its long eruptive history began ~100 ka ago (Gillot and Keller, 1993; Hornig-Kjarsgaard et al., 1993), and during this period Stromboli was several times the site of collapses whose magnitude varied in volume. Its most recent collapse history spans from the large sector collapse ($0.73 \pm 0.22 \text{ km}^3$, Tibaldi 2001) forming the Sciara del Fuoco (SdF) depression (Figure 1B) ~ 5 ka ago (Gillot and Keller 1993), to the submarine and subaerial flank failures involving a volume of ~20–30 × 10⁶ m³ and occurring along the same NW flank and triggering a tsunami

in 2002 (Bonaccorso et al., 2003; Tinti et al., 2005; Tommasi et al., 2005; Chiocci et al., 2008; Marani et al., 2009), to the further widening of the 2002 collapse scar after removing small rock volumes (~5 × 10⁵ m³; Falsaperla et al., 2006). Some of the lateral collapses that occurred during the Holocene triggered phreatomagmatic activity and pyroclastic density currents (PDCs) spreading along the flanks of the volcano (Lucchi et al., 2019). Crater-rim collapse PDCs occurred at the onset of flank eruptions (6 December 1985, 28 December 2002, 27 February 2007, 7 August 2014; De Fino et al., 1988; Pioli et al., 2008; Casagli et al., 2009; Di Traglia et al., 2018), or during lava overflows (12 January 2013, 6 August 2014, 19 May 2019; Calvari et al., 2016; Di Traglia et al., 2018). PDCs in historic times expanded mainly along the SdF as a result of paroxysmal or major explosive activity (Rittmann 1931; Calvari et al., 2006, 2020, 2021; Giordano and De Astis, 2021), but also because of small summit cone collapses caused by dike injection and magma fingering (Calvari et al., 2005, 2016). As an example, the 28 December 2002 PDC that reached the coastline, was generated by the sliding of the hot spatter fall deposit accumulated over the steep SdF slopes (Calvari et al., 2005; Landi et al., 2006; Pioli et al., 2008). Albeit rarely, PDCs can also spread outside the SdF. This occurred at least three times in the last century, during the paroxysms of 1906, 1930 and 1944 (Rittmann, 1931; Di Roberto et al., 2014; Salvatici et al., 2016), when small-volume flows of hot pyroclastic material spread on the West flank above the village of Ginostra, on the North flank within the Vallonazzo valley, and on the SE flank within the Forgia Vecchia, respectively (Figure 1B). In the latter two cases the PDCs reached the coast of the island.

The crater terrace is located at ~ 750 m elevation in the uppermost part of the SdF collapse depression (Figure 1B) and comprises three crater zones (Figure 1C): the NE crater zone (NEC), the central crater zone (CC), and the SW crater zone

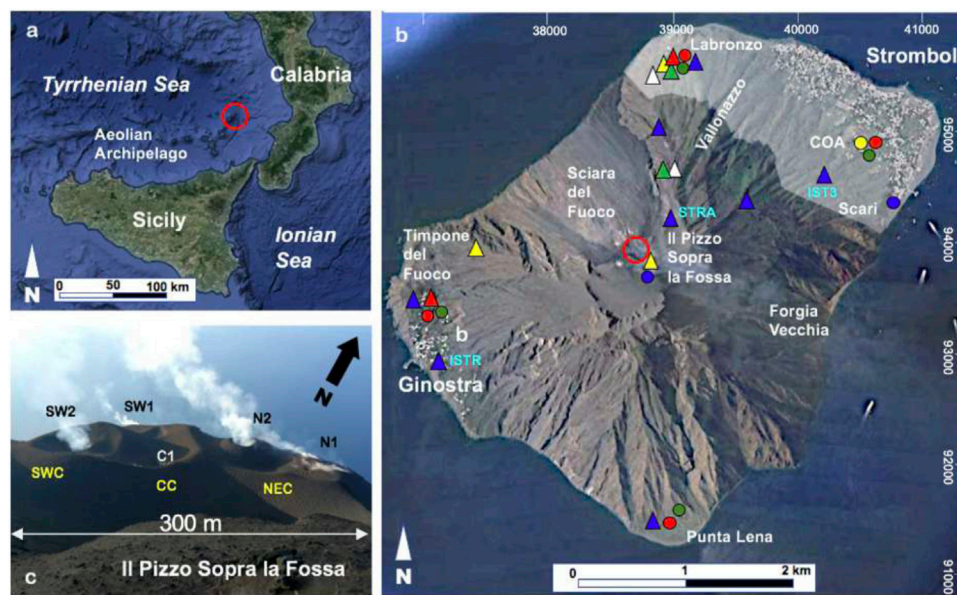


FIGURE 1

(A) GoogleEarth satellite imagery (7 July 2019) of southern Italy comprising Sicily, Calabria, the Aeolian Archipelago, with the position of Stromboli volcano marked by the red empty circle. (B) GoogleEarth satellite imagery (7 July 2019) of Stromboli island with the summit craters shown by the red empty circle, and indicating the distribution of the monitoring instruments used in this paper: yellow triangles: thermal cameras; white triangles: visible cameras; green triangles: GBInSARs; red triangles: tiltmeters; yellow circle: strainmeter; blue triangles: seismic stations; red circles: GNSS stations; green circles: FLAME stations for SO_2 measurements; blue circles: soil CO_2 monitoring stations. The light shaded area in the NE side of the island identifies the deposit of 19 May 2021 ash cloud. (C) Photo of Stromboli taken by Francesco Ciancitto on 13 January 2020 from Il Pizzo Sopra la Fossa, showing from the South the whole crater terrace (the field of view is ~ 300 m wide), the summit crater zones (SWC, SW crater zone; CC, central crater zone; NEC, NE crater zone) and the active vents C1, N1, N2, SW1 and SW2.

(SWC). Although the crater zones have been remarkably constant in position for more than a century (Washington, 1917; Rittmann 1931; Harris and Ripepe, 2007), they contain a variable number of active vents (Figure 1C) as a function of magma level within the conduit (Spampinato et al., 2008) and of the intensity of the eruptive activity (Civico et al., 2021). It is now recognized that any increase in magma level within the shallow feeder conduit results in an increasing number of explosion quakes (Martini et al., 2007), in a greater seismic tremor amplitude (Ripepe et al., 2009), in a greater number of explosions per hour detected from the monitoring thermal cameras (Calvari et al., 2010) and higher heat flux detected from satellites (Coppola et al., 2012; Corradino et al., 2021a; Ganci et al., 2021), in the inflation of the summit cone revealed by the GBInSAR devices (Di Traglia et al., 2018), and, in general, in morphology changes sometimes related to the shifting of the degassing activity and thermal anomaly within the crater terrace (Marotta et al., 2015). In turn, a higher magma level within the conduit causes magmatic pressure growth, and consequential increased possibility of a new summit cone failure (Di Traglia et al., 2020).

Since the end of the 2007 flank eruption (Patané et al., 2007; Neri and Lanzafame 2009), the summit crater terrace depression grew mainly on its NE margin building up a thick talus by

accumulation of debris, spatter and ejecta erupted during the persistent explosive activity by the NEC vents (Harris and Ripepe, 2007; Di Traglia et al., 2020; Schmid et al., 2021; Tioukov et al., 2022). This rapidly grown constructional morphology is also frequently affected by small collapses ($\sim 10^4$ – 10^5 m^3 ; Falsaperla et al., 2006; Civico et al., 2021). These collapses can be triggered by: 1) dike intrusion and magma fingering in between the loose breccia comprising the cinder cone (Acocella and Tibaldi, 2005; Calvari et al., 2016); 2) magmatic pressure increase when the magma level within the conduit increases (Di Traglia et al., 2018); or 3) by powerful major explosions such as the 16 November 2020 event (Calvari et al., 2021). In addition, the opening of eruptive fissures and/or vents along the SdF slope can result in instabilities of portions of the slope (Calvari et al., 2005, 2010), increasing the number of landslides (Martini et al., 2007; Falsaperla et al., 2006, 2008). The drainage of the shallow conduit may produce summit collapses and graben (Neri and Lanzafame, 2009) changing the capacity of the shallow feeder conduit and resulting in a greater number of major explosions and increased output rate (Coppola et al., 2012; Calvari et al., 2014; Civico et al., 2021).

The most recent eruptive activity at Stromboli was characterized by two powerful paroxysmal explosive episodes occurring on 3 July and 28 August 2019 (Giudicepietro et al.,

2019; Inguaggiato et al., 2019; Giudicepietro et al., 2020; Inguaggiato et al., 2020; Calvari et al., 2021; Giordano and De Astis, 2021; Inguaggiato et al., 2021; Giudicepietro et al., 2022) with a lava flow output starting on 3 July and ending on 30 August 2019 (Andronico et al., 2021). Both paroxysms of 3 July and 28 August were characterized by the ejection of gas-rich, low porphyritic LP magma of deep origin rising up quickly along the conduit (Métrich et al., 2005; Bertagnini et al., 2011; Plank et al., 2019; Giordano and De Astis, 2021; Métrich et al., 2021). The paroxysms gave rise to 5–6 km high eruptive columns, that collapsed and formed PDCs spreading along the SdF and on the sea surface, causing 2 m high tsunami waves on the coast of Stromboli (Aiuppa et al., 2021; Andronico et al., 2021; Giordano and De Astis, 2021). After the 2019 eruption crisis, the eruptive activity shifted again to the persistent Strombolian activity from the summit craters, punctuated by several major explosions and short-lasting, small-volume lava overflows from the summit craters, sometimes accompanied by crater failure and PDCs spreading along the SdF slope (Calvari et al., 2020; Corradino et al., 2021a; Aiuppa et al., 2021; Calvari et al., 2021).

In this paper, we analyze the events occurring at the volcano between 1 December 2020 and 30 June 2021 from a multi-disciplinary point of view. The data presented here comprise the sequence of the events gathered from the analysis of the thermal and visible images detected by the INGV monitoring camera network, and a quantification of the phenomena obtained from the camera network, helicopter photos, a drone survey, and satellite data, completed with the petrology of the erupted products. Multi-disciplinary geochemical and geophysical data involving the geochemistry of the SO₂ plume released from the summit craters and of the CO₂ released from the soils at the base of the volcano, seismicity, and ground deformation measured with different devices (GBInSARs, tilt, strainmeters and GNSS) and at various distance from the conduit (see Figure 1 and Supplementary Material), will be analyzed in an integrated way to discover precursors of the upward movement of magma within the shallow conduit, useful for hazard assessment. All times given in the paper are in UTC time.

2 Materials and methods

In this paper, we used several multi-disciplinary monitoring data from devices installed at Stromboli by the Istituto Nazionale di Geofisica e Vulcanologia (INGV) and by the Università di Firenze (Uni-FI). These comprise: a network of visible and thermal cameras, a seismic network, two GBInSAR devices, a GNSS network, three tiltmeters, one strainmeter, and a network for the measurement of SO₂ flux from the summit craters and of CO₂ flux from the ground. The network of visible and thermal cameras enabled characterizing and quantifying the eruptive activity occurring at the summit craters, and these results

were compared with thermal data gathered from satellites that allow a better and more complete view of the effusive phases. Photos taken by a helicopter survey carried out soon after the 19 May 2021 crater collapse, and the morphology profile obtained through a drone survey, allowed us to quantify the lost and gained volumes at the summit craters. Very-high-resolution multi-spectral and optical satellite imagery and radar images were used to map the distribution of the deposit on the flank of the volcano caused by the crater collapse and to estimate the covered area, its thickness and volume. Selected ash samples were collected during a field survey carried out on 19 May 2021 (the sampling area is shown in Figure 1B), immediately after the crater collapse, for characterizing their features, such as grain size distribution, components, and compositional analyses. These were compared to samples from the 28 December 2002 hot avalanche and of the 30 December 2002 SdF collapse.

The ground CO₂ degassing network was successfully used to monitoring changes in volcanic activity, showing a positive correlation between volcanic activity level and CO₂ fluxes (Inguaggiato et al., 2011; Inguaggiato et al., 2017; Inguaggiato et al., 2018; Inguaggiato et al., 2019; Inguaggiato et al., 2020). The geophysical devices are useful to detect any perturbation of the volcano that might evolve into a significant eruptive activity. In particular, seismicity changes according to the intensity of the explosive activity, to the magma level within the conduit, and to the variation of the eruptive style. The GBInSARs, GNSS network, tiltmeters and strainmeter allowed quantifying the ground deformation of the volcano recorded at varying distances from the summit, at different elevation, (see Figure 1B for the distribution of the devices on the flanks of the volcano), and at different timing. The position of the instruments used in this paper is shown in Figure 1B, and the details on the methods used for data analysis are fully described in the Supplementary Material (SM).

3 Results

3.1 Eruptive activity

The eruptive activity of Stromboli was quantified on the basis of the images recorded by the SCT thermal camera located at Labronzo (Figure 1B and Supplementary Material, Supplementary Table SM. 1) and by the MODIS satellite data, given that the SPT summit thermal camera located at Il Pizzo Sopra La Fossa—usually used for the automatic count of explosive activity—was destroyed in 2019 and not replaced until June 2021. Thus, the eruptive activity between 1 December 2020 and 30 June 2021 was detected from the SCT camera, which offers a NE side view of the craters. The eruptive activity automatic count is shown in Figure 2, where the results obtained from the SCT camera, in terms of explosion

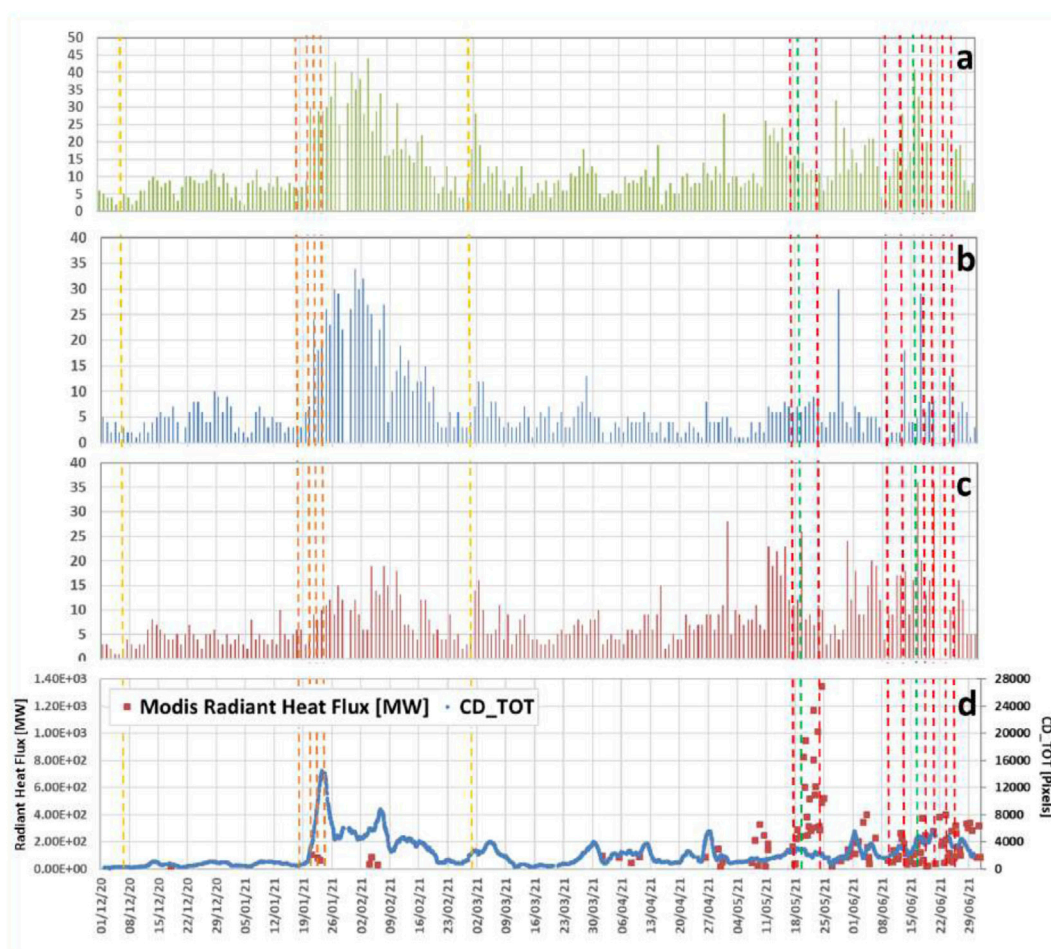


FIGURE 2

(A–C) Trend of explosive activity at the summit craters of Stromboli volcano detected from the INGV monitoring cameras between 1 December 2020 and 30 June 2021. (A) Green histogram: total number of explosions per hour detected from all the summit vents vs. time. (B) Blue histogram: number of explosions detected from the NE crater zone vs. time. (C) Red histogram: number of explosions detected for the SW and CC crater zones vs. time. (D) Radiant heat flux time series (red squares) retrieved from MODIS data at Stromboli volcano during 1 December 2020–30 June 2021 vs. the size of explosions (blue line) retrieved from the SCT camera and expressed as number of pixels (CD TOT). The vertical dashed lines show the main phases of eruptive activity listed in Table 1: yellow, major explosion; orange, spattering and/or overflows from the summit vents; red, lava flows along the Sciara del Fuoco; green, failure of the summit cone and pyroclastic density current (PDC) along the Sciara del Fuoco.

numbers per hour for the different crater zones (Figures 2A–C), are compared with the satellite-retrieved MODIS radiant heat flux data and with the Cumulative Dispersion (CD) obtained from the SCT camera (Figure 2D), which represents a rough estimate of the mass of the material ejected during each explosion (Mattia et al., 2021). The results from the SCT camera are displayed as total number of explosions per hour (Figure 2A), number of explosions per hour from the NEC crater zone (Figure 2B), and number of explosions per hour from the SWC and CC crater zones (Figure 2C). The graphs in Figure 2 show two phases of increased explosive activity, the first occurring between mid-January and mid-February 2021, and the second between early May and end of June 2021 (Figure 2A). The first phase was related to an increase of

explosive activity mainly occurring at the NE crater zone (Figures 2A,B), whereas the second phase was characterized by an increase in explosive activity especially at the SW and CC crater zones (Figures 2A,C).

The fire radiative power (FRP) time series, an estimation of the radiant heat flux, retrieved from VIIRS-SUOMI, VIIRS-NOAA and SLSTR-SENTINEL 3 for the time interval December 2020–June 2021 are shown in Figure 3. The maximum intensity in the investigated time interval was reached on 19 May 2021 at 12:54, with a value of 1.9 GW retrieved from VIIRS-SUOMI (Figure 3A). In fact, the VIIRS-SUOMI acquisition time was right after the start of the 19 May 2021 event, thus providing the closest estimate to the maximum radiative power generated during the collapse and lava flow

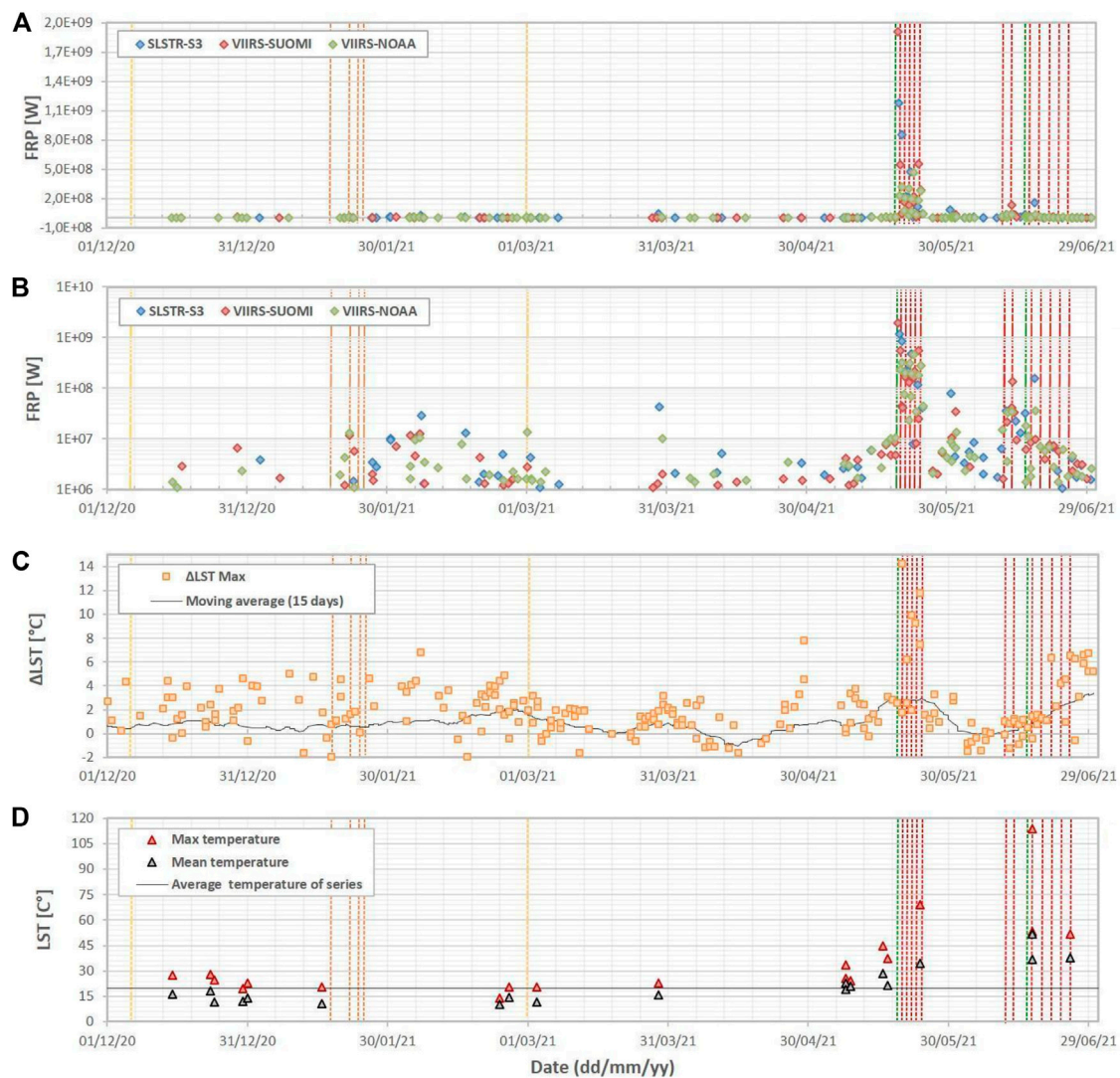


FIGURE 3

Thermal anomalies at Stromboli volcano from 1 December 2020 to 30 June 2021 using SLSTR and VIIRS to estimate FRP (A–B), MODIS to estimate temperature above average (Δ LST) (C), ASTER, L8 and ECOSTRESS to estimate LST at higher spatial resolution (D). FRP time series retrieved from SLSTR-SENTINEL 3 (blue diamond), VIIRS-SUOMI (red diamond) and VIIRS-NOAA (green diamond) at Stromboli volcano during 1 December 2020–30 June 2021 in linear scale (A) and log-scale (B). (C) Δ T_{max} retrieved from MODIS for each scene (orange squares) and its 15-days moving average (black line). (D) Temporal series of LST estimations by ASTER, L8 and ECOSTRESS data on summit craters. Mean and maximum temperatures in the considered area are reported; timing of major events are also depicted. The vertical dashed lines show the main phases of eruptive activity listed in Table 1: yellow, major explosion; orange, spattering and/or overflows from the summit vents; red, lava flows along the Sciara del Fuoco; green, failure of the summit cone and pyroclastic density current (PDC) along the Sciara del Fuoco.

output. Due to the skewness of the linear scale towards peak values, variations are not clearly visible in Figure 3A. We then used a logarithmic-scale to show FRP changes over time associated with volcanic activity phases (Figure 3B). A first activity phase was observed between December 2020 and March 2021 with a peak on 6 February 2021. A second brief phase was observed at the end of March 2021 with a peak on 29 March 2021. This was then followed by an increase in thermal activity on 7 May 2021, leading to the maximum on 19 May 2021.

Then, after a first drop, the thermal activity maintained a mid/high thermal level with peaks on 13 June and 17 June 2021, mirroring the trend obtained from the camera network (Figures 2A–C).

The temperature above average is the difference between what is observed and what is expected. We define Δ LST_{max} as the maximum value of Δ LST for each scene, and plotted its trend in Figure 3C. Δ LST_{max} low frequency trend was computed using a 15-days moving average showing the main volcanic

TABLE 1 List of the main volcanic events between 1 December 2020 and 30 June 2021 at Stromboli volcano detected by the monitoring cameras. The INGV monitoring reports are available at www.ct.ingv.it.

Date	Crater and vents	Activity	Starting time UTC	Ending time UTC	Duration	Size, and/or magnitude and/or intensity	References																																																																																																																											
6 December 2020	CC + SWC	Intense explosion, two pulses, 300 and 200 m high ash plumes, 2 PDCs along the SdF	05:12:44	05:12:54	10 s	VLP Size = 12,778 (normalized counts) Strain values =Duration: 5'15" Peak-peak amplitude: 14.5 ne	SCT Calvari et al. (2021) ; INGV report N50/2020																																																																																																																											
			05:13:41	05:14:06	25 s			18 January 2021	NEC (N1-N2)	Spattering from N2 and overflow from the saddle between N1 and N2	10:04	11:56	01:52		SCT	18 January 2021	NEC-N2	Spattering and overflow from N2, mainly blocks detaching from the front and rolling down slope for a few 100 s	14:53	22:30	07:37		SCT	22 January 2021	NEC	Overflow	11:22	20:00			INGV Rep. N° 4/2021	24 January 2021	NEC	Intense explosion followed by landslides	16:57			VLP Size = 2,810 No strain	INGV Rep. N° 4/2021	24–25 January 2021	NEC	Overflows	18:56 (24 January)	12:00 (25 January)			INGV Rep. N° 4/2021	1 March 2021	NEC+SWC N2	Major explosion	01:32:46	01:35:58	3.5 min	VLP Size = 11,684 Strain values = Duration: 4'53" Peak-peak amplitude: 16.6 ne	INGV Rep. N° 10/2021	19 May 2021	NEC N2	Failure NEC + PDCs	12:45	01:35:58		VLP Size max (3:30) = 3,996 Strain values =Duration: 60'00" Peak-peak amplitude: 14 ne		19–24 May 2021	NEC N2	Lava flow	12:45					11 June 2021	NEC N2	Lava flow	14:38					13 June 2021	NEC N2	Lava flow	02:04	03:04				16 June 2021	NEC N2	Failure + PDC	13:28					17 June 2021	NEC N2	Lava flow from eruptive fissure	19:10					19 June 2021	NEC N2	Lava flow from eruptive fissure	17:15					21 June 2021	NEC N2	Lava flow	04:05		04:10			23 June 2021	NEC N2	Lava flow						25 June 2021	NEC N2	Lava flow
18 January 2021	NEC (N1-N2)	Spattering from N2 and overflow from the saddle between N1 and N2	10:04	11:56	01:52		SCT																																																																																																																											
18 January 2021	NEC-N2	Spattering and overflow from N2, mainly blocks detaching from the front and rolling down slope for a few 100 s	14:53	22:30	07:37		SCT																																																																																																																											
22 January 2021	NEC	Overflow	11:22	20:00			INGV Rep. N° 4/2021																																																																																																																											
24 January 2021	NEC	Intense explosion followed by landslides	16:57			VLP Size = 2,810 No strain	INGV Rep. N° 4/2021																																																																																																																											
24–25 January 2021	NEC	Overflows	18:56 (24 January)	12:00 (25 January)			INGV Rep. N° 4/2021																																																																																																																											
1 March 2021	NEC+SWC N2	Major explosion	01:32:46	01:35:58	3.5 min	VLP Size = 11,684 Strain values = Duration: 4'53" Peak-peak amplitude: 16.6 ne	INGV Rep. N° 10/2021																																																																																																																											
19 May 2021	NEC N2	Failure NEC + PDCs	12:45	01:35:58		VLP Size max (3:30) = 3,996 Strain values =Duration: 60'00" Peak-peak amplitude: 14 ne																																																																																																																												
19–24 May 2021	NEC N2	Lava flow	12:45																																																																																																																															
11 June 2021	NEC N2	Lava flow	14:38																																																																																																																															
13 June 2021	NEC N2	Lava flow	02:04	03:04																																																																																																																														
16 June 2021	NEC N2	Failure + PDC	13:28																																																																																																																															
17 June 2021	NEC N2	Lava flow from eruptive fissure	19:10																																																																																																																															
19 June 2021	NEC N2	Lava flow from eruptive fissure	17:15																																																																																																																															
21 June 2021	NEC N2	Lava flow	04:05		04:10																																																																																																																													
23 June 2021	NEC N2	Lava flow																																																																																																																																
25 June 2021	NEC N2	Lava flow	14:25																																																																																																																															

eruption phases (Figure 3C). In particular, this parameter allowed us to detect the first phase of increased activity, that reached its peak in the second half of February 2021. The second phase of increased trend started on 10 April 2021 where an increase in ΔT was observed until the 19 May 2021 eruptive event. It is worth noting that a slight increase in the low frequency signal started on 17 April 2021, becoming steeper on 7 May 2021,

thus 12 days before the 19 May 2021 episode. A final sharp increase was observed from 11 June 2021 onwards, associated with the lava flow emission (Table 1). Moreover, LST time series by ASTER, Landsat8 and ECOSTRESS data were obtained by analyzing 19 nighttime images with no solar irradiation effects. In Figure 3D, mean and maximum temperatures on the crater's area are reported for the period 1 December 2020–30 June 2021.

In the first part of the LST time series, there are no significant variations in the mean temperature values; enhancements of mean and maximum temperatures are evident in the first half of May, just before the failure event on 19 May. During this period, maximum temperatures up to 45°C were estimated. After the failure event, we obtained a maximum temperature of about 75°C due to the presence of the lava flow. Intense lava flows that occurred also from 11 June were detected by satellite data acquired on 17 and 25 June, with mean temperatures of about 40°C and maximum temperatures up to 114°C.

On 6 December 2020, a stronger than usual explosion occurred (Table 1), that was classified as major on the basis of the VLP size (Giudicepietro et al., 2019), although some of the volcanological parameters allowed rating it more as an explosion of intermediate intensity than as a major event (Calvari et al., 2021). A Strombolian activity of average intensity was observed during January 2021 (Figures 2A–C). This activity was recorded by the MODIS satellite on 7 January, and between 21 and 24 January 2021 (Figure 2D). Four lava overflows occurred from the NEC crater rim on 18, 22 and 24 January 2021, and intense explosions on 24 January 2021 (Table 1). It is worth noting that in Table 1 and in the figures comparing multi-disciplinary data we distinguish between overflows (small lava flows covering the rim of the craters and travelling a few tens of meters, indicated in orange) from lava flows (indicated in red), which are larger lava outputs spreading for hundreds meters from the breached crater rim at high rate.

During the effusive phases, the average number of explosions increased reaching ~20 events/hour by the end of January (Figure 2), and the N2 vent produced lava fountaining reaching more than 100 m in height especially on 4 February 2021, when also the radiant heat flux was detected from satellite (Figure 2D). The explosive activity decreased slightly during the second and third weeks of February, and no radiant heat flux from MODIS was detected during the second half of February and March (Figure 2D). On 1 March, a powerful explosive sequence culminated with a major explosion at the NEC (Table 1), after which the explosive activity returned to medium-low levels (Figure 2) for the rest of March and the first half of April 2021, with a slightly increasing number of explosions from the end of April to mid-May (Figure 2). Moderate to low values of radiant heat flux were detected during the first half of April from MODIS, while an increase up to 330 MW was measured during 8–10 May and from 16 May onwards. After this, the satellite-derived radiant heat flux continuously grew, showing a sharp jump on 19 May when it reached the maximum value of about 1 GW. These higher values were recorded until the evening of 24 May. During June, moderate values were observed. The cumulative dispersion retrieved from the thermal camera data, measuring both the intensity and frequency of the explosion, is in agreement with the satellite-derived radiant heat flux during the intense spattering activity, while the two measurements did not match during the

effusive activity because the lava flows are better imaged by the satellite (Figure 2D).

On 19 May, an intense spattering activity was taking place from the NEC vents (Figures 1C, 4A,4B), when at 12:05 a more intense sequence of explosions caused the abundant fallout of bombs that rolled along the SdF and reached the sea, causing a dust cloud then blown backwards by the wind all along the slope. Spattering and bomb fallout along the slope continued, testifying to an increasing amount of magma being released from the crater rim when suddenly, at 12:50:32 the North flank of the N2 collapsed (Figure 4C). This produced a pyroclastic density current (PDC) that spread along the SdF (Figures 4D,E) with a speed of ~50 m s⁻¹ (estimated from the camera), reached the coastline and expanded on the sea surface for more than 1 km from the coast (Figures 4F–H). From the collapse scar of the summit crater a lava flow emerged at ~13:08, spreading along the SdF slope and reaching the coast in 43 s, at a speed of ~39 m s⁻¹. After the first PDC, several others occurred of decreasing size up to 13:35, while the number of explosions decreased after this episode (Figure 2) as a consequence of the upper conduit drainage. On 16 June (Table 1), a new failure of the NEC caused a PDC that spread on the upper SdF for several hundred meters.

From the photos taken during a helicopter survey carried out immediately after the failure (Figures 5A,B), we were able to estimate the volume of the block that collapsed from the North flank of the NEC. It was ~35 m high, ~60 m wide and ~40 m thick, giving an approximate volume of ~8.4 × 10⁵ m³. From the thermal survey, carried out with a drone on 21 September 2021 (Figures 5C–F), a prevalent activity was evident in the central area and in the SW (Figure 5E). This survey also highlighted the morphological change of the crater area with respect to both to what was observed from a helicopter survey after the 19 May 2021 collapse (Figure 5C) and in August 2021 (Figure 5D), and with what was detected on 20 June 2020 by Civico et al., 2021 (Figure 5F). In particular, by superimposing the NNE-SSW profiles obtained from the drone survey, the accumulation and erosion sectors are clearly distinguished (Figure 5F). The profile growth was maximum at the SWC with up to 20 m of accumulation (a3 in Figure 5F), whereas at the NEC we observed a maximum thickness increase of ~12 m (a2 in Figure 5F), and ~10 m of erosion at the CC (e2 in Figure 5F). This confirms that spatter accumulation around the NEC, caused by the persistent Strombolian activity, has partially rebuilt the summit cone, as can be observed by the comparison between the photos collected immediately after the failure (Figure 5C) and 3 months later (Figure 5D).

The SVO strainmeter recorded variations (Figure 6), related to the major explosions reported in Table 1, where we indicated the time durations and peak-to-peak amplitudes. The first explosion (Figure 6A) on 6 December 2020, took place in a noisy period. It was preceded by strain changes occurring several seconds before the explosion onset, and was characterized by a

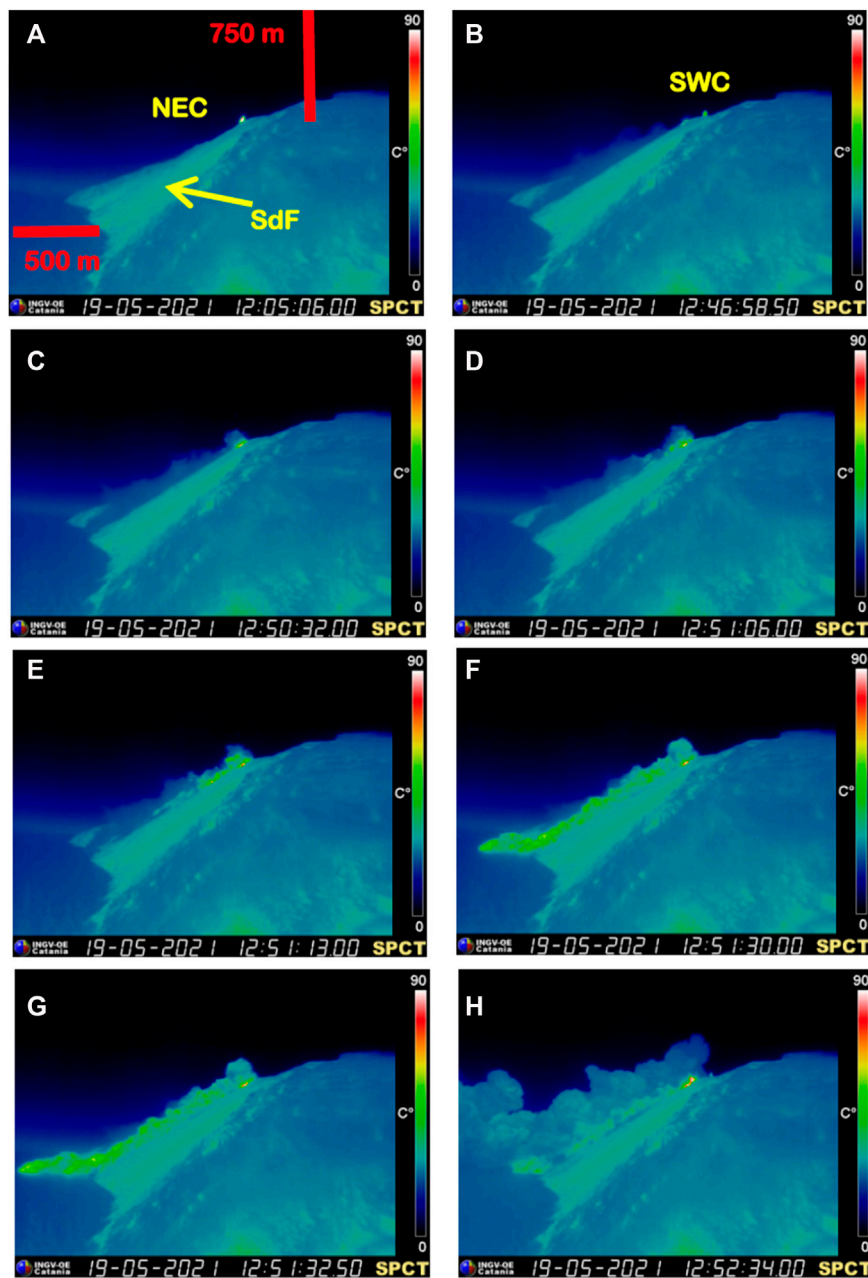


FIGURE 4

Thermal images from the SPCT monitoring camera with a view from the West flank of the Sciara del Fuoco of the sequence of NEC failure on 19 May 2021 at ~12:51. The temperature scale between 0 and 90°C is on the right of each frame. **(A)** Strombolian explosion from the NEC occurred at 12:05:06, with vertical and horizontal scales of the image displayed in red—note that at this stage the Sciara del Fuoco slope (SdF) was clean; **(B)** Strombolian explosion from the SWC occurred at 12:46:58—at this stage the SdF slope was affected by a dust cloud (in blue in the image) extending from the NEC to the coast; **(C)** overflow from the NEC triggering an initial failure of the crater flank at 12:50:32; **(D)** a hot avalanche or pyroclastic density current (PDC) started from the NEC due to the failure of the crater flank at 12:51:06; **(E)** the PDC spread along the SdF reaching half way along the slope at 12:51:13; **(F)** the PDC started spreading on the sea surface for ~300 m distance from the coast at 12:51:30; **(G)** the PDC traveled ~500 m on the sea surface at 12:51:32.50; **(H)** dust and steam cloud caused by the PDC entering the sea and the lava flow spreading along the SdF slope spread upwards towards the craters at 12:52:34.

transient which quickly dampened after the occurrence of the explosion. The second explosion on 1 March 2021 (Figure 6B) was accompanied by higher frequencies: in this case a single onset

was less clearly identifiable, and the explosion itself comprised several discrete explosions, which altogether gave rise to the eruptive event, whose cumulative energy was higher than that

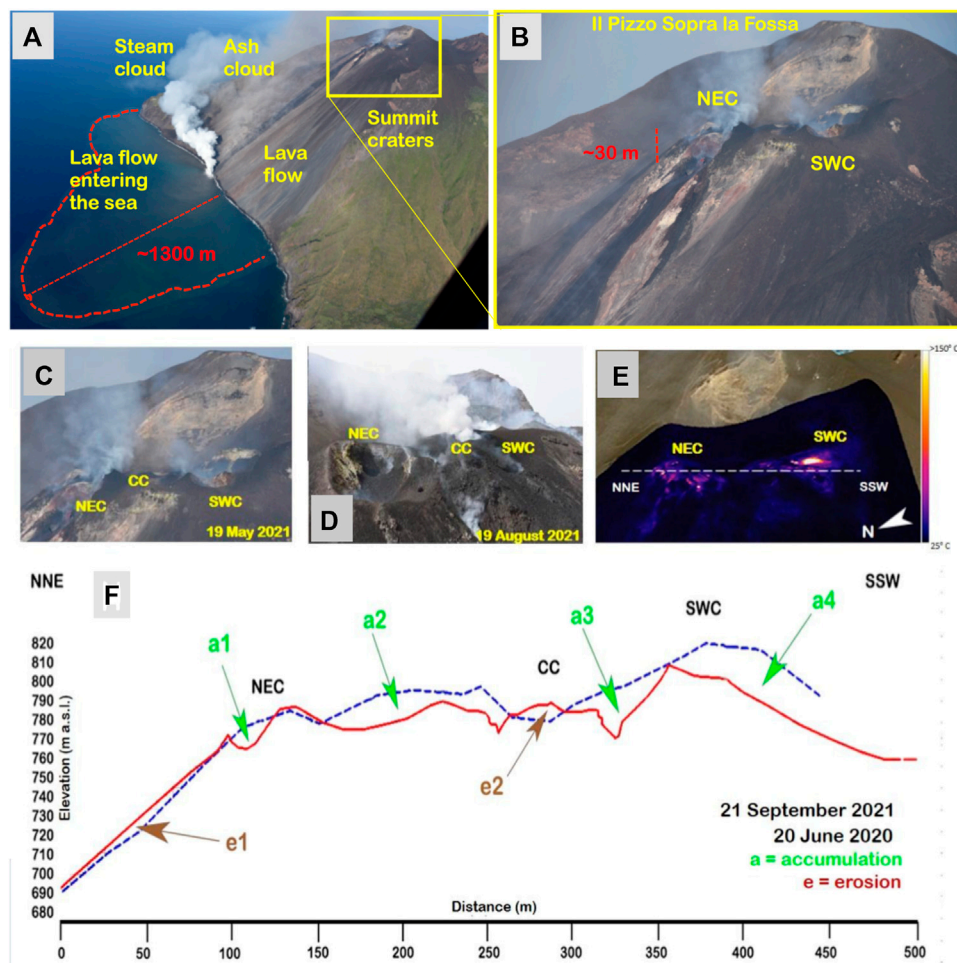
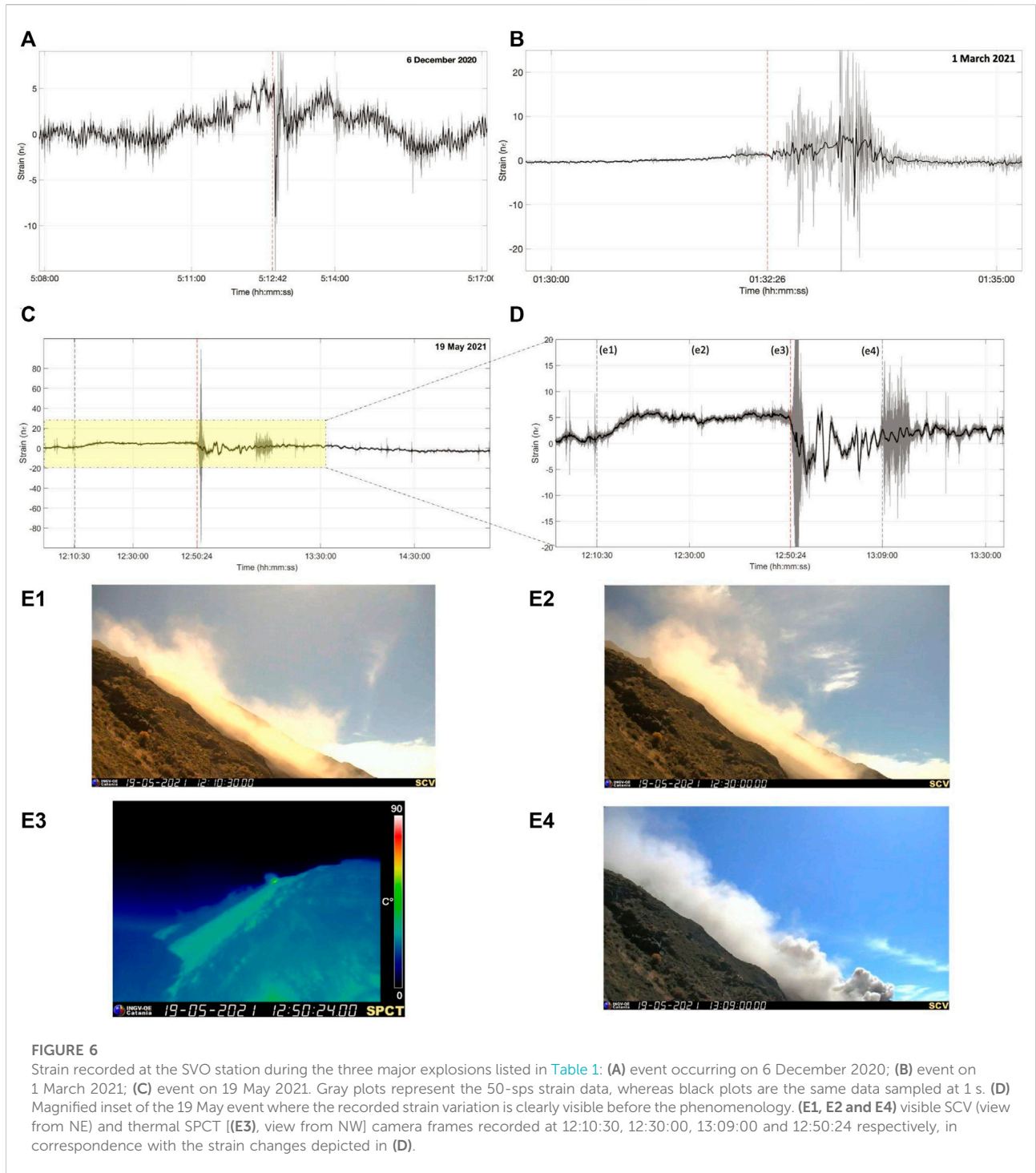


FIGURE 5

(A,B) Photos by Stefano Branca taken during a helicopter survey on 19 May 2021 immediately after the occurrence of the NEC failure and pyroclastic density current. (A) View from NW of the Sciara del Fuoco slope and summit craters of Stromboli, showing (in black) the lava flow discharged from the NEC North rim spreading along the slope and entering the sea where it gave rise to a thick white steam cloud, together with the light brown ash cloud rising along the slope due to the passage of the pyroclastic density current (PDC). The red dotted line on the sea surface shows the area affected by the expansion of the PDC up to a distance of ~1,300 m from the coast. (B) Close-up view of Stromboli summit craters from NW, displaying the area of the NEC failed during the 19 May 2021 collapse, that removed an estimated thickness of ~30 m. The position of the SWC is also shown. (C–D) Comparison between photos taken by helicopter surveys carried out (C) immediately after the 19 May 2021 collapse and (D) in August 2021, and (E) with a thermal mapping taken by UAV on 21 September 2021 to show the morphological changes of the summit region; (F) comparison between the cross section of the crater terrace along a profile NNE–SSW of September 2021 (blue dotted line) with that of June 2020 by Civico et al. (2021; red line), where e1 and e2 indicate erosion zones, a1–a4 indicate accumulation zones. The position of the summit crater zones are also indicated, with NEC, NE Crater zone; SWC, SW crater zone; CC, Central crater zone. The horizontal field of view of the images (C–F) is about 500 m.

dissipated by the previous episode. Finally, the last explosion occurring on 19 May 2021 (Figure 6C) was the most powerful of this period, presenting a more complex mechanism. The major explosion onset was preceded, about 40 min before (Figure 6D), by an inflation which had a step-like shape characterized by the beginning of a continuous uprise of dust along the Sciara del Fuoco (Figure 6E1, E2). The dust was caused by the rolling of blocks along the slope, possibly due to bombs fallout and/or lava flows covering the crater rim. This dust cloud was observed until 12:50:24 (Figure 6E3, where it appears blue in the thermal image),

when the sudden strain deflation concomitant with the major explosion was recorded. A sudden strain deflection was associated with the start of the major explosion, followed by consecutive inflections and deflections for almost 9 minutes. High frequency events (Figure 6E4) appeared after 18 min and were accompanied by several lower frequency oscillations, probably due to conduit resonance. A similar behavior was seen after the three paroxysmal events recorded by the same sensor in 2007 and 2019 (Di Lieto et al., 2020), then the strain re-equilibrated to the previous level.



3.2 Features of the volcanoclastic deposits

We used Sentinel-1 SAR amplitude data to map volcanic deposits related to the 19 May 2021 event. The 16 May 2021 was considered as a pre-eruptive image, and the 22 May 2021 as a post-eruptive image to compute the ratio amplitude image

(Figure 7). From the four ratio amplitude images (Figures 7A–D), the cumulative volcanic deposits were retrieved (Figure 7E) using the procedure for Sentinel-1 SAR amplitude images with spatial resolution of 10 m described in Corradino et al. (2021b), resulting in a total area extent of 107,600 m².

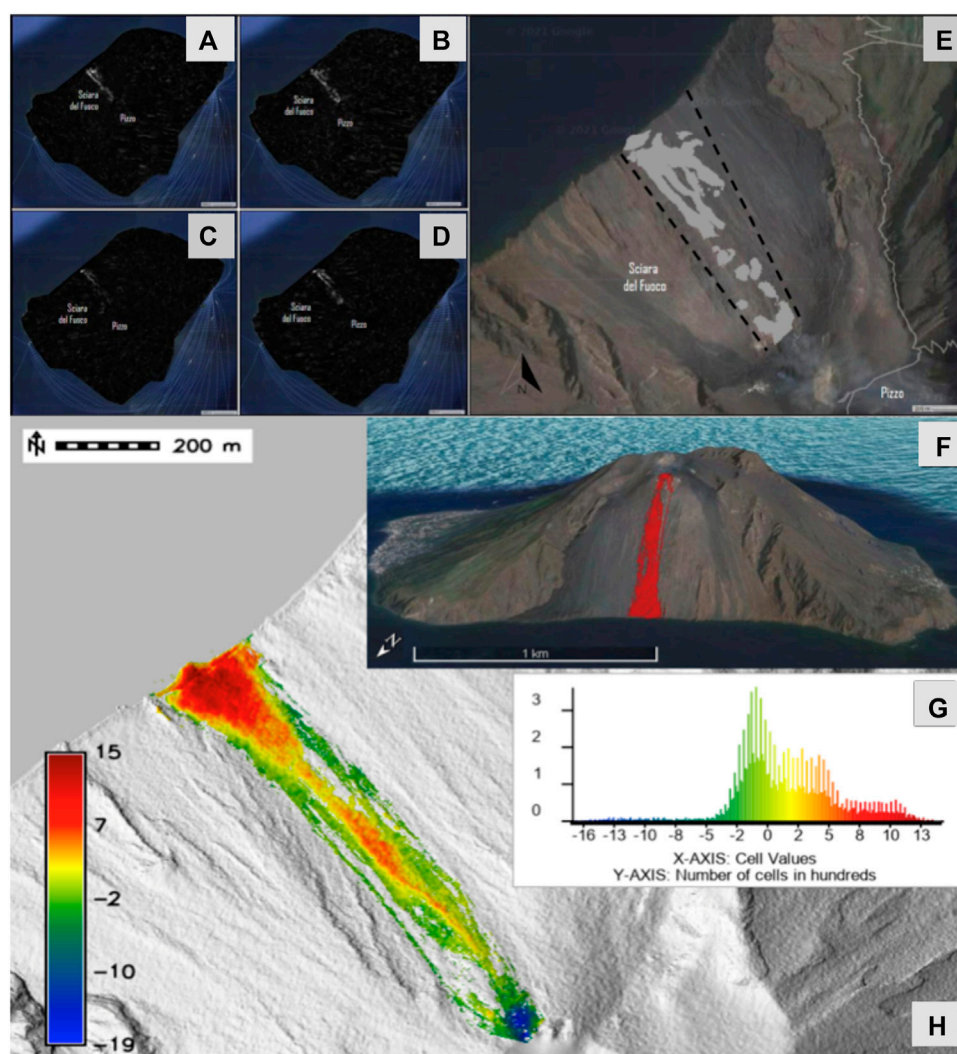
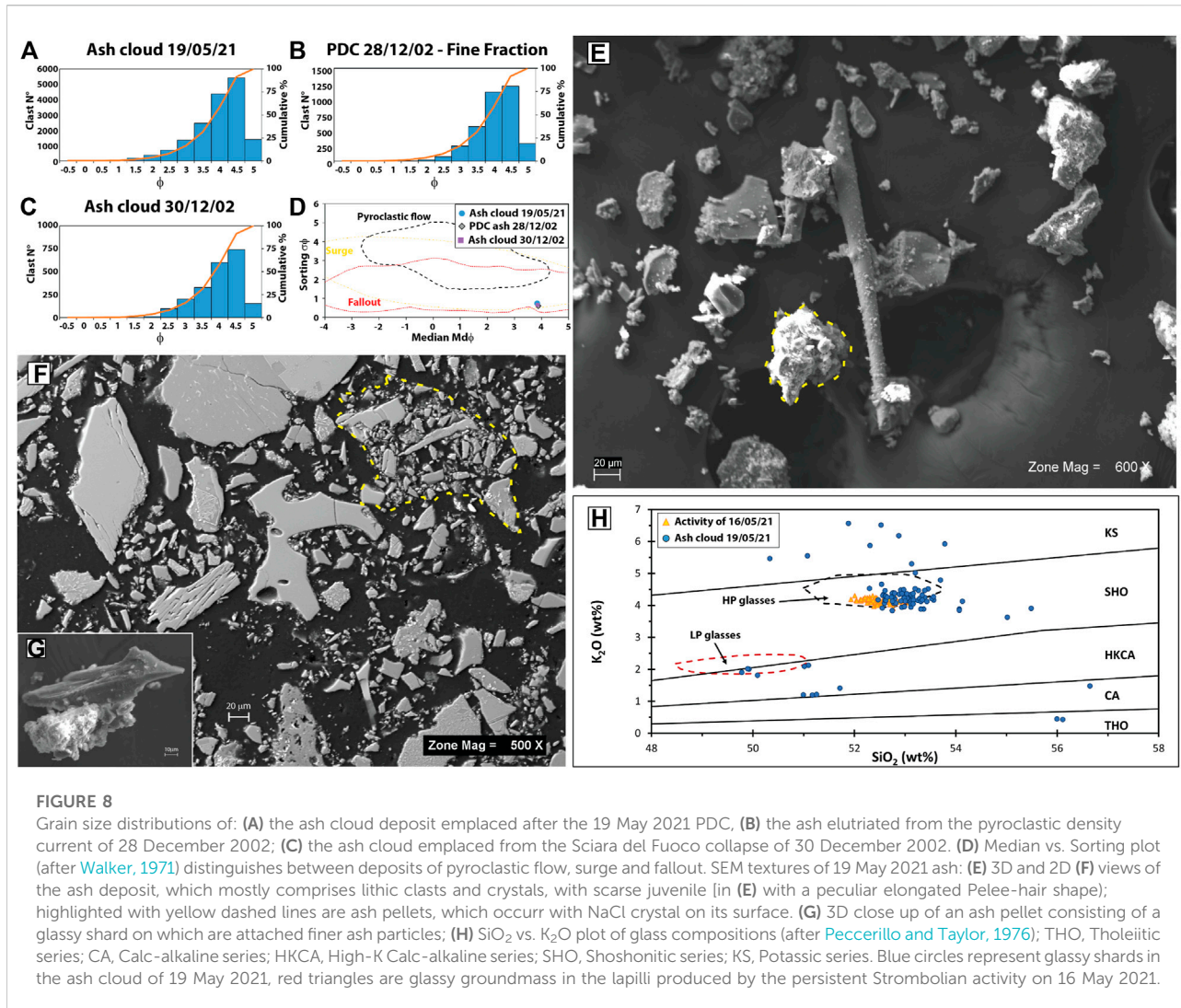


FIGURE 7

Volcanic deposits retrieved from Sentinel-1 SAR amplitude image rationing considering the 16 May 2021 as a pre-eruptive image, and the 22 May 2021 as a post-eruptive image. Descendent orbits are shown in (A) with VV-polarization and (B) VH polarization; ascent orbits are shown in (C) with VV-polarization and (D) VH polarization. Cumulative volcanic deposits are retrieved from the four ratio amplitude images and shown in gray in (E). The two black dotted lines in (E) mark the boundaries of the deposit. (F) Google Earth view of the Skysat-derived deposits spreading along the Sciara del Fuoco. (G) Thickness distribution of the DEM residuals. (H) 3D mapping of the deposits inside the Skysat-derived area. Colors of the legend represent the deposit thickness in meters.

The detailed quantification of the volcanic deposits emplaced during the May-June 2021 eruptive activity was also performed thanks to the availability of very-high-resolution multi-spectral and optical satellite imagery (i.e., Skysat and Pléiades). Using the Skysat Collect product acquired on 21 May 2021 at 09:40, we performed a preliminary 2D mapping of the deposit area, which was $124,750 \pm 11,410 \text{ m}^2$ (Figure 7F). This estimate was complemented by analyzing the distribution of the deposits through a topographic approach, i.e., by subtracting pre- and post-eruptive Digital Elevation Models (DEMs; Ganci et al., 2018; Ganci et al., 2019). Both

DEMs were obtained by processing two tri-stereo Pléiades images, acquired on 8 May and 4 June 2021. From the residuals of the DEM difference, we obtained the distribution shown in Figure 7G. The thickness of volcanic deposits ranges from -19 m , due to the crater-rim collapse, to 15 m , in proximity to the coast (Figure 7H). The area with negative thickness measured about 40% ($54,200 \text{ m}^2$) of the total area, leading to an erosion volume of $122,140 \pm 32,525 \text{ m}^3$. The volume of the deposits amounts to $305,380 \pm 42,325 \text{ m}^3$. This comprises both the PDCs of the 19 May 2021 collapse and the lava flowing from the breached crater rim. Uncertainty in



volumes was estimated by multiplying the areas by the residual vertical accuracy outside the deposits.

The 19 May ash cloud settled as a continuous layer of very fine (dusty) unconsolidated ash, pinkish to purplish in color, with thicknesses less than 1 mm, on the entire eastern side of the island (the dispersion area is annotated in Figure 1B). Calculated values of weight normalized on sampling area (g/m^2) displayed a scattered distribution on the field, ranging from 18.31 to 145.38 g/m^2 , therefore unrelated to the distance from the source. The grain size distribution (GSD) revealed that all the collected samples were characterized by a great abundance of fine-grained clasts, even below the lower limit of 5 ϕ and under the analytical resolution. Within the measured size interval, the GSD showed a log-normal trend, with Md_ϕ of around 3.8. All the samples are overall moderately sorted with a σ_ϕ around 0.74 (Figure 8A). For comparison, the GSDs of the ash elutriated during two episodes of the 2002 eruption are shown: the hot

avalanche of 28 December and the landslides occurring since 30 December (Figures 8B,C). Both samples display very similar curves, and in the Md_ϕ vs. σ_ϕ diagram (Figure 8D; after Walker, 1971) all of them cluster in a very narrow space within the field of fallout.

The 19 May ash cloud deposits comprised different components, including pumices, glass shards, and lithics mainly made of lava fragments and altered clasts (Figures 8E,F). Finer clasts often aggregate in ash pellets with a fairly regular rounded outline up to 500 μm (Figures 8E–G). 3D imaging of ash pellets reveals the presence of sodium chloride (NaCl) crystals on their surface (Figure 8G), suggesting the involvement of seawater steam in their formation. There are a multitude of dense clasts with different microphenocryst contents in a holocrystalline groundmass, that are interpreted as lava fragments. Many others are reddish to yellowish clasts, altered by the hot gasses or recycled within the craters. There is

also a great abundance of loose crystals. A small amount of pumices (up to 350 μm) having angular to sub-rounded morphology and sharp edges, and volcanic glass shards are also present. Morphologies range from dense and blocky to spongy and moderately vesicular with spaced and non-collapsed bubbles. Textures are porphyritic with scarce micro-phenocrysts (plg + cpx + ol) or aphyric, and the groundmass is glassy with scarce microlite of swallow-tailed plagioclase. These components are interpreted as juvenile material.

Major element composition of glass measured in the latter category shows a large variability on the SiO_2 vs. K_2O diagram, ranging from HKCA basalt to shoshonite (Figure 8H; Peccerillo and Taylor, 1976). Most of the compositions cluster within the fields of high-porphyritic (HP; Francalanci et al., 1999) glasses erupted during the recent activity of Stromboli, and in particular overlap the composition of the magma erupted during the ordinary Strombolian activity of 16 May 2021. Few glasses plot within the field of low-porphyritic (LP; Francalanci et al., 1999) composition. Some others are more scattered and exhibit higher and lower content of K_2O , respectively. High- K_2O glasses could derive from Neostromboli products. Low values of K_2O and Na_2O suggest significant glass alteration.

3.3 Gas geochemistry and geophysics

In order to compare the information deriving from the seismic measurements with the temporal evolution of the eruptive activity of Stromboli in the target period, we calculated the time series of seismic amplitude and VLP (very long period) size of STRA data, a seismic station installed close to the craters and near Il Pizzo Sopra la Fossa (Figure 1B; additional details are in the Supplementary Material, and in Supplementary Table SM. 2). The seismic amplitude and VLP size are sensitive to changes in the intensity of the ordinary Strombolian explosive activity and the variation of the eruptive style, respectively (Giudicepietro et al., 2019; Calvari et al., 2021; Giudicepietro et al., 2021). The hourly rate of VLPs, on a daily basis, and the daily rate of landslide signals that are routinely monitored were also considered. By comparing these parameters with the volcanic events reported in Table 1, we found that the two explosions stronger than usual, occurring on 6 December 2020 and 1 March 2021 respectively, with the second classified as a major explosion on the basis of most parameters (Table 1), did not show particular variations of the seismic parameters considered here, which had low values (Figure 9). The phase characterized by spattering and small lava overflows at the end of January 2021 was anticipated by an increase in the VLP size, but by less significant changes in the other seismic parameters (Figure 9). Conversely, the crater collapse and consequent PDC episode of 19 May 2021, which was the most significant event to occur in the period considered here, was preceded by an increase in the VLP size and the seismic

amplitude, recognizable a few days before the event (Figure 9). The effusive activity at the end of June 2021 was also preceded by an increase in all the seismic parameters, including the VLP/hour and landslide signals.

While Figure 9 shows the measurements of the seismic amplitude in a station located in the summit of the volcano, we also analyzed seismic waveform data from two broadband stations from the Italian National Seismic network operating at Stromboli: IST3 and ISTR, located respectively at Stromboli and Ginostra (Figure 1B). These stations are located in distal areas and close to other instruments for geophysical and geochemical monitoring. The instrument response was removed to obtain the 3-component ground motion (both displacement and velocity). The seismic records were then filtered in the VLP (2–30 s) and tremor (1–3 Hz) frequency bands. Finally, the RMS (root mean square) amplitude in these frequency bands was computed in 10-minute-long windows (Figure 10A). Looking at the seismic amplitude in the VLP frequency band, long term changes in both the RMS amplitude and in the variance of the measurements in both stations can be observed. Such time series was compared with sea level data from two gauges (Strombolicchio and Ginostra) recorded by the Istituto Superiore per la Protezione e la Ricerca Ambientale (ISPRA), indicating that periods of time with high RMS amplitude and low variance of measurements are mostly correlated with large sea level variations probably associated with storm surges (Figure 10A). On the other hand, we note that the RMS amplitude in the tremor band follows similar patterns to those observed in the summit station and shown in Figure 9C, that is, a clear increase in the seismic amplitude around both February and May 2021.

The GNSS data from the 1 December 2020 to 30 June 2021 showed short phases of areal dilatation that characterize the deformation pattern of the island. The dilatation is evidenced in Figure 10B, which shows the variation of the area recorded at the triangle STDF-SVIN-SPLN that contains the crater area. The time series started at the end of February 2021 because the station SPLN worked intermittently before that date. Areal dilatation is measured between 13 and 19 March 2021, 5 and 8 April 2021 and also between 11 and 16 May 2021. To investigate the deformation pattern before the end of February 2021, we analyzed the time series of the length variations between the stations STDF and SVIN that cross the crater area (Figure 1B). It shows a lengthening between 22 January and 6 February 2021 and also during the phases of areal dilatation highlighted in Figure 10B. The lengthening is due to areal dilatation.

In the same period, each variation of the long trend strain signal recorded at SVO site has a slight correlation with the barometric pressure as shown in Figure 10C; hence the strain signal can be associated with changes in the weather and sea conditions.

Figure 10D displays the TDF tilt signals recorded between December 2020 and June 2021. The TDF sensor is at a constant

temperature, thus the signals have low noise, not showing seasonal effects related to temperature as at the PLB station. In the first period, the tilt showed a slow and continuous down vector toward the summit craters. Since the beginning of May, the tilt showed a trend change indicating uplift toward the SdF. The 15 May change indicated a lowering tilt (of about 2.0 microradians) toward the summit area.

The investigated period was characterized by an oscillatory trend of deformations detected by the GBInSAR, with periods characterized by ground displacements at the limit of the instrument's measuring capacity, by periods of inflation (displacements towards the sensors), and periods of rapid deflation (displacements away from the sensors). In Figure 10E, it is possible to note the trend of both the cumulative and daily displacements in the area of the crater terrace measured by the GBInSAR NE190, that having a wider Field-Of-View (FOV), allows characterizing the deformation in a wider area. There was an initial period (1 November 2020–25 December 2020), featuring low displacements (on average 0.6 mm/day towards the sensor), followed by a period of acceleration that culminated on 24 January 2021 (on average 6.9 mm/day towards the sensor), followed by a strong deflation which lasted until the 26 January 2021 (about 16.4 mm/day away from the sensor). The deflation coincided with a series of overflows that occurred on 24–25 January 2021, also associated with intense explosive activity, with fountaining and spattering in the crater terrace. After this deflation, there was a new inflation (on average 7.8 mm/day towards the sensor) until 19 February 2021. Subsequently, a new period with low deformations occurred (about 1 mm/day towards the sensor) until the 31 March 2021, followed again by inflation (on average 2.6 mm/day towards the sensor) which lasted until 19 May 2021, and which initiated a series of deflation/inflation lasting until the end of the investigated period. The first deflation occurred between 19 and 28 May 2021 (7.4 mm/day away from the sensor), following the lava flow that was generated by a vent located on the edge of the crater terrace and which opened after the NEC crater-rim collapse. This event was followed by inflation until 18 June 2021 (7.5 mm/day towards the sensor), a new deflation until the afternoon of 19 June 2021 (35 mm/day away from the sensor). The deflation coincided with a series of overflows between 17 and 19 June 2021. Subsequently, the last inflation/deflation cycle took place, with the peak approaching the sensor reached on the morning of 25 June 2021 (11 mm/day towards the sensor), at which time the recorded movements were away from the sensor (7.6 mm/day).

The soil CO₂ fluxes recorded at the STR01 station, in the peripheral area of Scari located on the active fault trending N41°E (Finizola et al., 2002), showed during the 7 months of observation an anomalous degassing above the average value (100 g m⁻² d⁻¹) with values of 150 g m⁻² d⁻¹ in December 2020 and a strong and sharp increase of fluxes starting in May 2021. It reached about 300 g m⁻² d⁻¹ in June, the highest

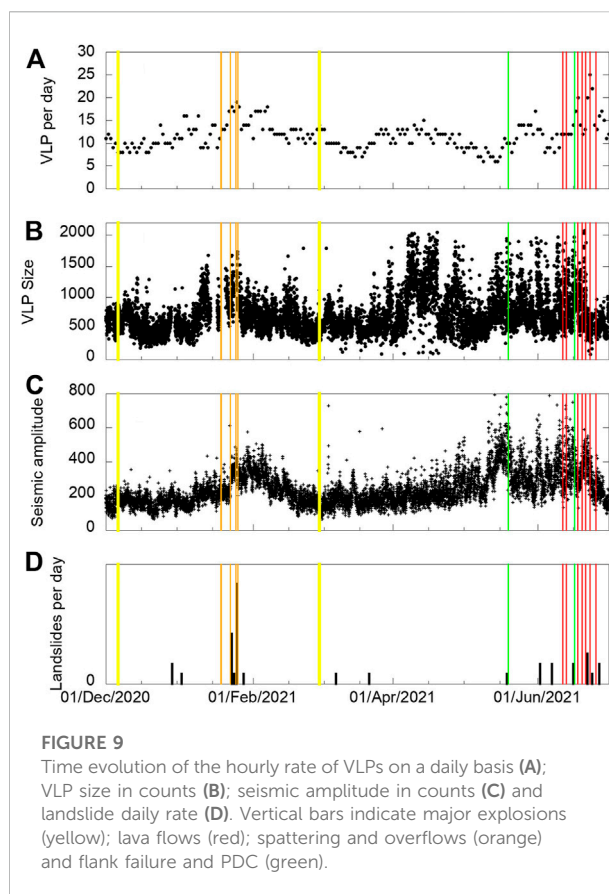


FIGURE 9
Time evolution of the hourly rate of VLPs on a daily basis (A); VLP size in counts (B); seismic amplitude in counts (C) and landslide daily rate (D). Vertical bars indicate major explosions (yellow); lava flows (red); spattering and overflows (orange) and flank failure and PDC (green).

values ever recorded for this area during the last 15 years of observation (Figure 10F). A similar behavior was observed in the bulk SO₂ flux from November 2020 to June 2021, but the peaks of SO₂ flux were delayed by ~2 weeks when compared to the peaks of CO₂ flux (Figures 10E,F). Specifically, over the 7 months taken into account here, the SO₂ flux signal displayed a general increase spread into two waxing-waning stages, each lasting ~100 days of mean duration, in which the flux gradually increased to peak at high values between 300 and 460 t/d. Both increased stages encompass the intense eruptive activity occurring in January and May 2021 (Figure 2).

4 Discussion

The aim of this study was to characterize the preparatory phase of the volcano that started on December 2020 and led to the May–June 2021 eruptive activity. In addition, we seek to verify if it is possible to distinguish from the monitoring signals in advance any small batch of magma rising up along the feeding system from a much more voluminous supply like the one leading to the 2019 eruptive phase, which was fed by gas-rich low-porphyrific (LP) magma

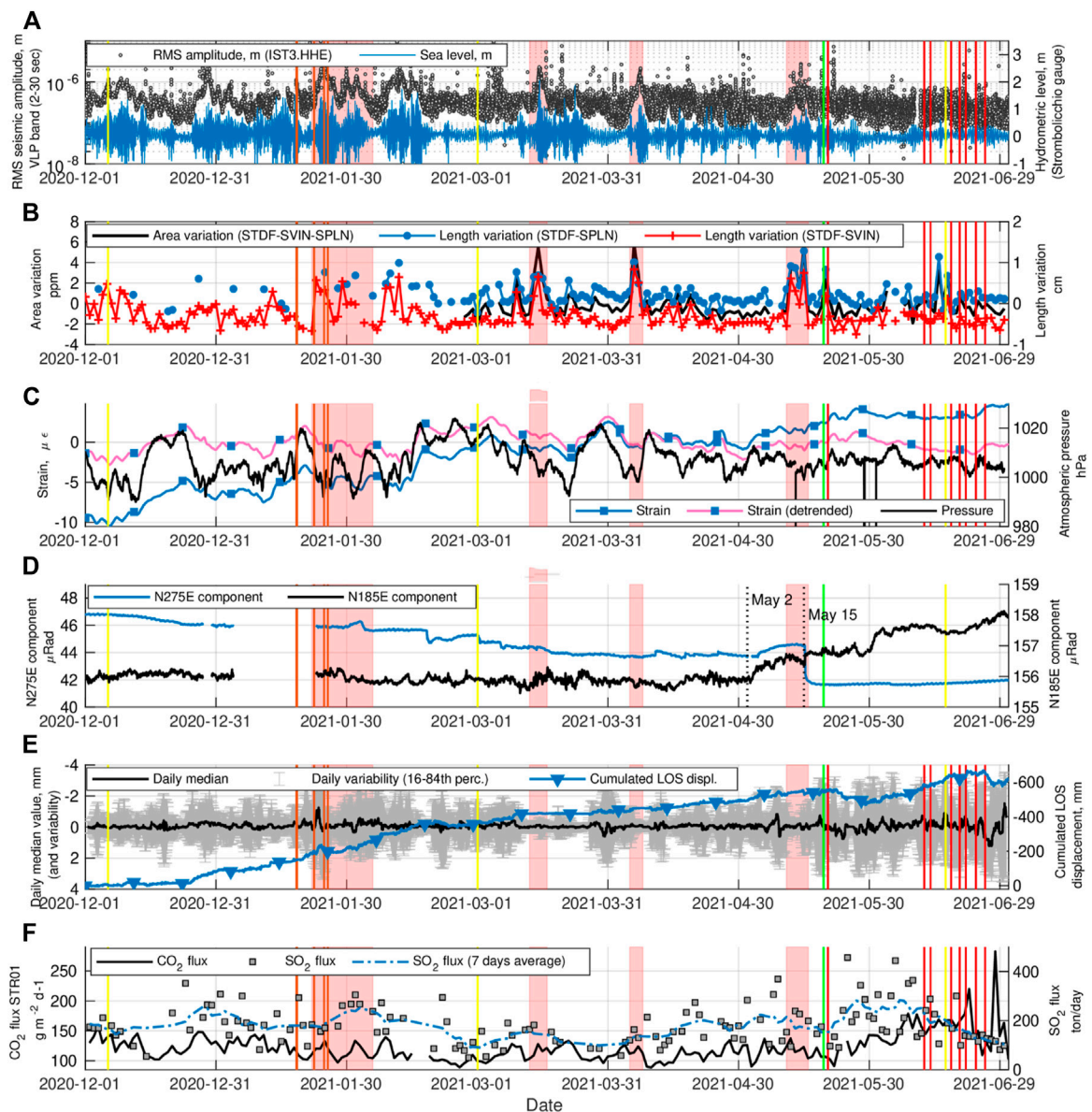


FIGURE 10

(A) RMS amplitude measured in the IST3 very broadband seismic station in the frequency band from 2 to 30 s (which includes the typical frequencies of VLP events at Stromboli). The blue line shows the sea hydrometric level measured at Strombolicchio gauge (sea level data from ISPRA). (B) Variation of the area recorded at the triangle STDF-SVIN-SPLN (black line) and variation of the baseline between the STDF-SPLN (blue points) and STDF-SVIN (red points) stations. The pink rectangles indicate short phases characterized by areal dilatation. (C) Raw and linear detrended strain (blue and red lines) and barometric pressure (black line) time series recorded at SVO station. (D) The two tilt components recorded at Timpono del Fuoco. From the beginning of May (first black dotted line) a change in the long-term trend is visible. The 15 May sharp variation is also evidenced by the black dotted line. (E) GBInSAR displacement time series: the blue line represents the cumulative displacement measured along the LOS; the black line represents the median (50th percentile) of the measures in a moving window of 24 h length, with a sampling step of 1 h; the Gy bars are the values of the 16th and 84th percentiles. In (F) the daily and 7-days average bulk SO₂ flux emitted from the summit craters of Stromboli (blue curve and gray blue squares, respectively) and the CO₂ flux from the soil at Scari area, STR01 station (black curve) are displayed. The vertical bars indicate major explosions (yellow); lava flows (red); spattering and overflows (orange) and flank failure and PDC (green).

(Andronico et al., 2021; Giordano and De Astis, 2021). For the analysis, we used ground-based and satellite remote sensing multi-parametric data. These results may have important

implications for hazard assessment at Stromboli volcano and may prove useful for other open conduit active basaltic volcanoes (Zago et al., 2017, 2019).

4.1 Unrest

The multi-parametric analysis of volcanic activity is a powerful tool to contemporaneously analyze multiple observations and to improve the interpretation of volcanic signals; for this reason it has become a key practice for volcano monitoring and for interpreting data during volcanic unrest (Garcia-Aristizabal et al., 2007; Bertolaso et al., 2008; Bonaccorso et al., 2015; Solana et al., 2017; Peltier et al., 2018). The thermal activity of Stromboli volcano was observed both by fixed thermal cameras and multispectral satellites. These two kinds of instrument are complementary, and the joint analysis of the two can improve the interpretation of both the signals. Indeed, due to cloud coverage, during winter only rarely could the eruptive activity be observed by satellites, while the most reliable information came from the ground. From MODIS, we measured an increase of the thermal activity during the first days of May and were able to follow the sequence of eruptive events thereafter. Conversely, by ground thermal camera data we managed to quantify the explosive activity in terms of number of explosions and cumulative dispersion, i.e., a rough estimate of the mass of the material ejected during each explosion. Comparing the two signals, i.e. ground thermal cameras and satellite, if the information derived from the cameras agrees with satellites, we are usually in the presence of intense spattering activity or low effusion rate lava overflows. When the thermal signal derived from satellite is much greater than that of the ground camera, this is probably due to sustained lava flows or PDCs, which can be detected only partially from our ground monitoring cameras due to the side view. When the thermal signal derived from satellite is much smaller than that of the ground camera, we experienced thick cloud coverage or small size explosions that are difficult to be detected from satellites.

The new unrest of the volcano was at first identified by the ground monitoring systems on 6 December 2020, when a bigger than usual explosion was recorded (Table 1). This episode was accompanied by a significant change in the VLP size and strain signals (Table 1; Figures 9, 10A), and caused the formation of two small PDCs along the SdF slope (Calvari et al., 2021). A gradual increase in the explosive activity at the summit craters was detected by the monitoring cameras between end of January and early February 2021 (Figure 2), being more pronounced at the NEC than at the SWC+CC (Figures 2B,C). Also the radiant heat flux from MODIS (Figure 2D), and the VIIRS-SUOMI, VIIRS-NOAA and SLSTR-SENTINEL 3 fire radiative power time series displayed a gradual increase of the signals, peaking on 6 February and 29 March 2021 (Figure 3), especially when overflows occurred from the crater rim (Table 1).

The phase characterized by spattering and small lava overflows at the end of January 2021 was anticipated by an increase in the VLP size, and by less significant changes in the other seismic parameters (Figure 9). Conversely, the two explosions on 6 December 2020 and 1 March 2021 (Table 1)

happened when the seismic parameters did not show particular variations and had low values (Figure 9). The output of overflows from the crater rim at the end of January was accompanied by an increasing rate of landslides occurring along the SdF (Figure 9D), as a result of the blocks detaching from the flow front and rolling down the slope, thereby triggering further landslides (Di Traglia et al., 2021; Zhou et al., 2022).

The ground deformation data detected through tilt, GNSS and GBInSAR revealed a growing effect of the magma level rising within the conduit that gradually moved from the instruments located at lower altitudes on the slope of the volcano (tilt and GNSS) to the GBInSAR located at higher elevation (Figures 10B–E). On the contrary, during the analyzed period, the strainmeter data showed negligible long-term variations, while short-term changes were recorded just before the three more energetic explosive events occurred, each one with its particular features (Table 1; Figure 6). The eruptive activity of May and June 2021 was anticipated by a number of intense and major explosions and by lava flows spreading along the SdF slope.

The 6 December 2020 event had the strain time-history of an explosion with a higher than usual amplitude (Figure 6A). The 1 March 2021 major explosion appeared to be formed by the overlapping of multiple explosions (Figure 6B). The most significant strain changes were observed for the 19 May 2021 event, when longer and more complex strain variations accompanied the volcano phenomenology (Figures 6C,D). Schematically, we recognized four phases: an hour before the PDC began, a strain increase suggested that the volcano system was in over-pressure (Figure 6E1); after 10 min the signal levelled off when a continuous spattering occurred from the summit craters (Figure 6E2); as soon as the PDC occurred, a sudden strain decrease took place (Figure 6E3); final longer oscillations suggested a conduit resonance due, probably, to its emptying (Figure 6E4).

The soil CO₂ flux measured at Scari (Figure 1B) from December 2020 to June 2021, was characterized by anomalous degassing values and showed a strong increase in May 2021 which peaked at the end of June at about 300 g m⁻² d⁻¹, (Figure 10F). This anomalous CO₂ flux value confirmed a long and continuously increasing trend begun in 2017 (Inguaggiato et al., 2020, 2021). This continuous increase in the CO₂ flux, mirrored by the SO₂ flux that was split into two cycles heralding the January-February and May-June effusive phases (Figure 10E), suggested pressurization of the conduit by gas-rich magma entering the supply system. According to the SO₂ flux data (Figure 10F), we suggest that the two cycles were caused by two distinct supplies of gas-rich magma that entered the plumbing system from November 2020. However, the two magma batches differ in both magnitude and mass emission rate over time. The first rose gradually and leveled-off at high values for ~50 days, feeding an intense explosive activity coupled with spattering and overflows (Figure 2 and Table 1), whereas the second grew more rapidly, reflecting a more sustained ascent of

fresh magma. Eventually, these batches pushed up the degassed HP magma residing in the upper conduit, causing the passive collapse of part of the summit cone and the lava flows occurring between 19 and 24 May 2021. It is worth noting that the two major explosions on 6 December 2020 and 24 January 2021 (Table 1) took place following a moderate decrease of the SO₂ flux. These temporal degassing changes suggest that more intense explosions might result from a partial sealing of the upper conduit which prevents or decreases the degassing, eventually leading to a pressurization of the top of the volcano conduit (Calvari et al., 2012; Salerno et al., 2018).

An interesting point of discussion arises by observing a good agreement between continuous geophysical measurements and the sea level data (Figure 10). Large sea level variations are mostly due to storm surges driven by weather perturbations, as evidenced by the low atmospheric pressure that accompanies such periods (Figure 10C). Storm surges can be tracked in the low frequency band of broadband seismic records (e.g., Bromirski et al., 1999; Ardhuin et al., 2015; Cannata et al., 2020; Cutroneo et al., 2021), as shown in the RMS ground motion displacements in the low frequency band in Figure 10A. It is worth noting however that such periods also show a good agreement with the periods in which the number of volcanic VLP events increases (Figure 9A), as well as with deformation measurements (as for instance, from GNSS, Figure 10B and the tilt change during the last period, Figure 10D). The obvious question arising at this point is: what is the nature of this correlation between volcanic activity and the external, weather related, perturbations? Is the volcanic system responding to external perturbations, or do the external perturbations influence the geophysical measurements? Patané et al. (2007) have already suggested the possible influence of external perturbations on Stromboli's magmatic system, observed at the onset of the 2007 eruption when severe weather conditions probably induced fluctuating stresses on the magmatic system and could have brought about eruptive activity variations. These phenomena seem particularly evident in volcanoes located in small islands surrounded by the sea. However, more detailed analyses would be needed to answer this question.

4.2 The collapse event, PDC and lava flows

Thermal anomalies have been monitored from space by using both the radiant heat flux and land surface temperature (LST) highlighting the main eruptive phases. Relevant changes have been observed before the 19 May 2021 event. In particular, increases in both FRP measured by VIIRS and SLSTR (nearly 12 days) and Δ LST measured by MODIS (nearly 1 month) anticipated this eruptive event (Figures 2, 3). The FRP estimate closest to the 19 May 2021, 12:45 event was acquired by VIIRS-Suomi with an estimate of 1.9 GW at 12:54 on 19 May 2021, providing the closest measurement to the

event. Volcanic deposits including emplaced lava flows, pyroclastic flows, ballistics and tephra fallout related to the event of 19 May 2021 have been mapped by using Sentinel 1-SAR amplitude data.

The volume removed from the crater area by the 19 May failure was estimated at $\sim 8.4 \text{ m}^3 \times 10^5 \text{ m}^3$ (Figure 5). Following the crater failure, a lava flow poured out from the breached crater rim spreading along the SdF slope and eroding the ground surface (Figure 7H). The resulting deposit was $\sim 305,380 \pm 42,325 \text{ m}^3$, comprising both the PDC and the lava flow from the breached crater rim. The area with negative thickness measured about 40% ($54,200 \text{ m}^2$) of the total area, leading to an erosion volume of $122,140 \pm 32,525 \text{ m}^3$. This erosion was clearly evident in the components of the ash released by the spreading of the PDC that comprised a large amount of lithic material (Figure 8F). The thickness distribution derived from Pléiades and Skysat satellite images acquired in May-June 2021 (Figure 7H) has shown volcanic deposits with increasing thicknesses going in a SE-NW direction from the crater to the coast. These include erosion (up to 19 m in thickness) near the crater, and emplaced deposits (up to 15 m in thickness) at the lava flow front. This kind of distribution was seen during other similar events at Stromboli, characterized by lava flows from the crater spreading along the SdF and reaching the sea (e.g. Calvari et al., 2020). The PDC spread along the SdF at a speed of $\sim 50 \text{ m s}^{-1}$ and expanded on the sea surface for more than 1 km from the coast (Figures 4G, 5A). Considering the small volume of the initial failure and its growth by erosion along the slope, as well as its speed, the effect on eventual mariners close to the coast could be extremely dangerous, especially given that these events occurred several times in the past without warning (De Fino et al., 1988; Pioli et al., 2008; Di Traglia et al., 2018; Calvari et al., 2021).

Ground deposition and distribution of the ash cloud is mainly controlled by the PDC path and by the cloud dispersal due to the wind direction. Grain size distribution is strongly skewed toward fine sizes (Figure 8). As expected, the shape of the clasts is mainly related to secondary fragmentation by comminution instead of being primary magmatic (Figure 8). The nature of the clasts reflects a juvenile component, a lithic fraction related to the ingestion of the material along the PDC path, and the aggregation processes related to the interaction of the hot material with the sea water. Similar features have been observed in deposits of the PDC taking place at the beginning of the 2002 eruption and in large tsunamigenic landslides occurring since the 30 December 2002. Glassy clasts, recognizable as juvenile, mainly reflect the composition of the HP magma feeding the ordinary Strombolian activity. The origin of few clasts showing the composition of LP magma is not clear; however we are inclined to interpret them as accidental lithics taken up during the transport along the SdF. Similarly, alkali-depleted exotic compositions observed in apparently fresh glassy clasts are attributable to alteration of the fine-grained material

that accumulated within and outside the crater, successively remobilized by the collapse. All the above features further confirm that collapse of the cone and erosion of the upper slope of the SdF are important phenomena to be considered for hazard assessment.

4.3 Hazard assessment

The images reported in [Figure 5](#) clearly display the growth of the summit cone as a result of the persistent explosive activity that characterizes the volcano. The drone survey carried out in September 2021, when compared to the previous profile obtained in June 2020 by [Civico et al. \(2021\)](#), shows several zones of growth and accumulation of erupted products around most of the summit vents ([Figure 5F](#)), involving an increased hazard of further failures. In addition, a recent survey detected a significant volume increase of the talus building up the NE flank of the summit cone ([Tioukov et al., 2022](#)), thus confirming the summit area of the volcano as being prone to further collapses.

Most of the vents that triggered the recent eruptive activity of Stromboli are aligned along a NE-SW direction, this being the outcome of the shallower portion of the magma intrusion marking the strike of the eruptive fissure ([Marsella et al., 2012](#)). As a consequence, lava emission from the NE side of the NEC can be considered the result of a dike intrusion, which breaches the crater rim and guides the lava flows along the lateral slope escarpments ([Marsella et al., 2012](#)). The growth rate of the summit craters, obtained by digital elevation model comparison between 2004 and 2006 and caused by the accumulation of products from the persistent Strombolian explosive activity, is estimated at $\sim 0.01 \text{ m}^3 \text{ s}^{-1}$ ([Marsella et al., 2012](#)). This compares to the slightly lower $\sim 0.008 \text{ m}^3 \text{ s}^{-1}$ obtained from the measurements of [Civico et al. \(2021\)](#), and to the $0.002 \text{ m}^3 \text{ s}^{-1}$ estimated by [Harris and Ripepe \(2007\)](#), against a steady rate of magma supply from depth estimated at $0.1\text{--}0.5 \text{ m}^3 \text{ s}^{-1}$ by [Harris and Stevenson \(1997\)](#) and at $0.3\text{--}0.6 \text{ m}^3 \text{ s}^{-1}$ by [Allard et al. \(1994\)](#).

It is interesting to note that effusive events, as well as more frequent/intense explosive activity, spattering and sporadic fountaining, all phenomena indicating high magma in the shallow feeding system of Stromboli, occurred after significant increases in deformations recorded by GBInSAR sensors. Similarly, the deflation that follows effusive events testifies to how emptying is limited to the shallowest feeding system. Contrariwise, the explosive events classified as “major” (Class 2 by [Calvari et al., 2021](#)), occurred in conjunction with periods of small deformations recorded by GBInSARs, at the limit of instrumental detection. All this would suggest that the explosive-effusive activity is controlled by an upward shift of the more superficial feeding system, which manifests itself in periods that can last weeks or months (as already evidenced by [Di Traglia et al. \(2014a\)](#), [Di Traglia et al. \(2014b\)](#), [Di Traglia et al. \(2015\)](#), [Calvari et al. \(2016\)](#), [Di Traglia et al. \(2018\)](#), [Calvari et al.](#)

[\(2021\)](#)), whereas the high intensity explosive transients are controlled by faster dynamics affecting the deep supply systems (as proposed by [Pichavant et al., 2022](#)). These results could be applied to other open vent volcanic systems displaying persistent or frequent explosive activity, such as Yasur (Vanuatu), Piton de la Fournaise (La Réunion), Shishaldin (Alaska), Fuego (Guatemala), Nyiragongo (R.D. Congo), Masaya (Nicaragua), Turrialba (Costa Rica), Etna (Italy), Kilauea (Hawaii), provided that a suitable monitoring system exists.

5 Conclusive remarks

The main points resulting from this study can be summarized as follows:

- The detection of mild eruptive activity from the ground and satellite shows differences and complementary aspects that may give important indications on the state of the volcano when analyzed in an integrated way.
- Major explosions and paroxysms are usually not preceded by detectable volcanological or geophysical parameters that might be useful for an early warning of this activity, but are immediately (a few minutes) preceded and accompanied by strain signals that allowed us to characterize the state of pressurization of the shallow supply system.
- Several parameters increased before the 19 May 2021 event of collapse and lava flow output, suggesting pressurization of the shallow conduit (a few hundred meters below the vents): MODIS and satellite heat flux, explosive activity detected from the monitoring cameras, GBInSAR, GNSS, Tilt, seismicity, strain, CO₂ flux, SO₂ flux. The upward movement of degassed batches of magma leading to effusive activity is normally slow enough to be detected in real time by the monitoring systems here considered.
- The 19 May 2021 failure was characterized by using: photos from a helicopter survey to estimate the collapsed volume ([Figure 5](#)); Sentinel-1 SAR ([Figures 7A–E](#)) to retrieve the area of the deposit along the SdF; Skysat ([Figures 7F–H](#)) for the volume and thickness of the deposit resulting from the collapse and lava flow output, obtaining an area of negative thickness $\sim 40\%$ ($54,200 \text{ m}^2$) of the total area, leading to an erosion volume of $122,140 \pm 32,525 \text{ m}^3$ over a total emplaced volume (only along the slope) of $305,380 \pm 42,325 \text{ m}^3$ comprising both the lava flow and the PDC; componentry and composition of the deposit ([Figure 8](#)). Much greater volumes are expected when also considering the amount of deposit emplaced below sea level for more than 1 km distance from the coast ([Figure 5A](#)).

- Comparison with the much more powerful 2019 eruptive phase: VLP Size and seismicity similar but lasting a shorter time; CO₂ flux increasing constantly as recorded since the end of the 2002-03 eruption; different velocity of the magma rising along the conduit, that can be detected in case of an effusive phase (slow) and cannot be detected in case of a paroxysmal explosion (very fast); petrology and timing of magma rising along the deep (10–12 km below sea level depth) and shallow (2 km depth to the vents) supply system; the GBInSAR accurately detects the deformation of the shallow supply system caused by the degassed magma entering the system, but does not record changes when gas-rich magma is rising fast triggering paroxysmal episodes.
- The composition of the 19 May 2021 deposit involved a large amount of lithics that matches the erosion of the crater area and SdF slope evidenced by the Skysat (Figure 7).
- Hazard assessment: the rapidity of growth of the summit cones after the 19 May 2021 failure makes this area prone to the possibility of new failures in the next future, and suggests that mariners should keep a safety distance of more than 2 km from the coast (Figure 7).

Key points

- Small volume summit failures can have major impacts on the surrounding areas
- Summit failure deposits can increase their volume by slope erosion
- Multi-disciplinary monitoring systems may help forecast slow and degassed magma batches rising along the conduit
- The supply of gas rich magma from the deep storage, triggering major explosions and paroxysms, is normally too fast to be detected by the monitoring systems.

Data availability statement

The raw data supporting the conclusion of this article will be made available by the authors, without undue reservation.

Author contributions

Conceptualization: SC, FD, GG, VB, BD, AG, FG, SI, PR, MM, MP, and GS; methodology: SC, FD, GG, VB, FC, BD, SG, AG, FG, SI, FV, MC, CI, GM, MMa, MMu, LM, TN, MP, PR, GS, NC, GR, PD, AD, AC, CC, EA, FT, CD, AE, WD, TC, MF, VR, MS, EM, RA, GA, and PB; data curation: all authors.

Funding

This research was funded by the Project FIRST-ForecastIng eRuptive activity at Stromboli volcano: Timing, eruptive style, size, intensity, and duration, INGV-Progetto Strategico Dipartimento Vulcani 2019 (Delibera n. 144/2020). This research was funded by the “Presidenza del Consiglio dei Ministri–Dipartimento della Protezione Civile,” through the UniFi-DPC 2019-2021 agreement (Scientific Responsibility: N.C.).

Acknowledgments

We would like to thank: the Editor in Chief, Valerio Acocella, the Editor handling the paper, TT, KN, and BH who carefully reviewed the paper and provided extremely useful suggestions to improve the structure and clarity of the paper; the Istituto Superiore per la Protezione e la Ricerca Ambientale (ISPRA) for the availability of the sea level gauge data reported in Figure 8A; Stephen Conway for revising the English style. The data used in this paper belong to INGV and can be made available upon request to the authors. The contents of this paper represent the authors’ ideas and do not necessarily correspond to the official opinion and policies of the “Presidenza del Consiglio dei Ministri–Dipartimento della Protezione Civile”.

Conflict of interest

The authors declare that the research was conducted in the absence of any commercial or financial relationships that could be construed as a potential conflict of interest.

Publisher’s note

All claims expressed in this article are solely those of the authors and do not necessarily represent those of their affiliated organizations, or those of the publisher, the editors and the reviewers. Any product that may be evaluated in this article, or claim that may be made by its manufacturer, is not guaranteed or endorsed by the publisher.

Supplementary material

The Supplementary Material for this article can be found online at: <https://www.frontiersin.org/articles/10.3389/feart.2022.899635/full#supplementary-material>

References

- Acocella, V., and Tibaldi, A. (2005). Dike propagation driven by volcano collapse: A general model tested at Stromboli, Italy. *Geophys. Res. Lett.* 32, L08308. doi:10.1029/2004GL022248
- Aiuppa, A., Bitetto, M., Delle Donne, D., La Monica, F. P., Tanburello, G., Coppola, D., et al. (2021). Volcanic CO₂ tracks the incubation period of basaltic paroxysms. *Sci. Adv.* 7, eabh0191. doi:10.1126/sciadv.abh0191
- Allard, P., Carbonnelle, J., Metrich, N., Loyer, H., and Zettwoog, P. (1994). Sulphur output and magma degassing budget of Stromboli volcano. *Nature* 368, 326–330. doi:10.1038/368326a0
- Andronico, D., Del Bello, E., D’Orsiano, C., Landi, P., Pardini, F., Scarlato, P., et al. (2021). Uncovering the eruptive patterns of the 2019 double paroxysm eruption crisis of Stromboli volcano. *Nat. Commun.* 12, 4213. doi:10.1038/s41467-021-24420-1
- Antonello, G., Casagli, N., Farina, P., Leva, D., Nico, G., Sieber, A. J., et al. (2004). Ground-based SAR interferometry for monitoring mass movements. *Landslides* 1 (1), 21–28. doi:10.1007/s10346-003-0009-6
- Arduhuin, F., Gualtieri, L., and Stutzmann, E. (2015). How ocean waves rock the Earth: Two mechanisms explain microseisms with periods 3 to 300 s. *Geophys. Res. Lett.* 42, 765–772. doi:10.1002/2014GL062782
- Bertagnini, A., Di Roberto, A., and Pompilio, M. (2011). Paroxysmal activity at Stromboli: Lessons from the past. *Bull. Volcanol.* 73, 1229–1243. doi:10.1007/s00445-011-0470-3
- Bertagnini, A., Coltelli, M., Landi, P., Pompilio, M., and Rosi, M. (1999). Violent explosions yield new insights into dynamics of Stromboli Volcano. *Eos Trans. AGU*. 80 (52), 633. doi:10.1029/99eo00415
- Bertolaso, G., Bonaccorso, A., and Boschi, E. (2008). “Scientific community and civil protection synergy during the Stromboli 2002–2003 Eruption,” in *The Stromboli volcano, an integrated study of the 2002–2003 eruption*. Editors S. Calvari, S. Inguaggiato, G. Puglisi, M. Rippepe, and M. Rosi (American Geophysical Union, Washington, D.C.: AGU Geophysical Monograph), 182, 387–397. doi:10.1029/143GM31
- Bonaccorso, A., Calvari, S., and Boschi, E. (2015). “Hazard mitigation and crisis management during major flank eruptions at Etna volcano: Reporting on real experience,” in *Detecting, modelling and responding to effusive eruptions*. Editors A. J. L. Harris, T. De Groeve, F. Garel, and S. A. carn (Geological Society, London, Special Publications), 426, 447–461. ISBN 978-1-86239-736-1. doi:10.1144/SP426.4
- Bonaccorso, A., Calvari, S., Garfi, G., Lodato, L., and Patané, D. (2003). Dynamics of the December 2002 flank failure and tsunamis at Stromboli volcano inferred by volcanological and geophysical observations. *Geophys. Res. Lett.* 30 (18), 1941–1944. doi:10.1029/2003GL017702
- Bromirski, P. D., Flick, R. E., and Graham, N. (1999). Ocean wave height determined from inland seismometer data: Implications for investigating wave climate changes in the NE Pacific. *J. Geophys. Res.* 104, 20753–20766. doi:10.1029/1999JC900156
- Burton, M. R., Caltabiano, T., Murè, F., Salerno, G., and Randazzo, D. (2009). SO₂ flux from Stromboli during the 2007 eruption: Results from the FLAME network and traverse measurements. *J. Volcanol. Geotherm. Res.* 182, 214–220. doi:10.1016/j.jvolgeores.2008.11.025
- Casagli, N., Tibaldi, A., Merri, A., Del Ventisette, C., Apuani, T., Guerri, L., et al. (2009). Deformation of Stromboli Volcano (Italy) during the 2007 eruption revealed by radar interferometry, numerical modelling and structural geological field data. *J. Volcanol. Geotherm. Res.* 182 (3–4), 182–200. doi:10.1016/j.jvolgeores.2009.01.002
- Calvari, S., Büttner, R., Cristaldi, A., Dellino, P., Giudicepietro, F., Orazi, M., et al. (2012). The 7 September 2008 Vulcanian explosion at Stromboli volcano: Multiparametric characterization of the event and quantification of the ejecta. *J. Geophys. Res.* 117, B05201. doi:10.1029/2011JB009048
- Calvari, S., Bonaccorso, A., Madonia, P., Neri, M., Liuzzo, M., Salerno, G. G., et al. (2014). Major eruptive style changes induced by structural modifications of a shallow conduit system: The 2007–2012 Stromboli case. *Bull. Volcanol.* 76, 841. doi:10.1007/s00445-014-0841-7
- Calvari, S., Di Traglia, F., Ganci, G., Giudicepietro, F., Macedonio, G., Cappello, A., et al. (2020). Overflows and pyroclastic density currents in march–april 2020 at Stromboli volcano detected by remote sensing and seismic monitoring data. *Remote Sens.* 12 (18), 3010. doi:10.3390/rs12183010
- Calvari, S., Giudicepietro, F., Di Traglia, F., Bonaccorso, A., Macedonio, G., Casagli, N., et al. (2021). Variable magnitude and intensity of strombolian explosions: Focus on the eruptive processes for a first classification scheme for Stromboli volcano (Italy). *Remote Sens. (Basel)*. 13, 944. doi:10.3390/rs13050944
- Calvari, S., Intrieri, E., Di Traglia, F., Bonaccorso, A., Casagli, N., Cristaldi, A., et al. (2016). Monitoring crater-wall collapse at active volcanoes: A study of the 12 January 2013 event at Stromboli. *Bull. Volcanol.* 78 (5), 39. doi:10.1007/s00445-016-1033-4
- Calvari, S., Lodato, L., Steffke, A., Cristaldi, A., Harris, A. J. L., Spampinato, L., et al. (2010). The 2007 Stromboli eruption: Event chronology and effusion rates using thermal infrared data. *J. Geophys. Res.* 115, B04201. doi:10.1029/2009JB006478
- Calvari, S., Spampinato, L., Lodato, L., Harris, A. J. L., Patrick, M. R., Dehn, J., et al. (2005). Chronology and complex volcanic processes during the 2002–2003 flank eruption at Stromboli volcano (Italy) reconstructed from direct observations and surveys with a hand-held thermal camera. *J. Geophys. Res.* 110, B02201. doi:10.1029/2004JB003129
- Calvari, S., Spampinato, L., and Lodato, L. (2006). The 5 April 2003 vulcanian paroxysmal explosion at Stromboli volcano (Italy) from field observations and thermal data. *J. Volcanol. Geotherm. Res.* 149, 160–175. doi:10.1016/j.jvolgeores.2005.06.006
- Campion, R., Delgado-Granados, H., and Mori, T. (2015). Image-based correction of the light dilution effect for SO₂ camera measurements. *J. Volcanol. Geotherm. Res.* 300, 48–57. doi:10.1016/j.jvolgeores.2015.01.004
- Cannata, A., Cannavò, F., Moschella, S., Di Grazia, G., Nardone, G., Orasi, A., et al. (2020). Unravelling the relationship between microseisms and spatial distribution of sea wave height by statistical and machine learning approaches. *Remote Sens.* 12 (5), 761. doi:10.3390/rs12050761
- Chiocci, F. L., Romagnoli, C., Tommasi, P., and Bosman, A. (2008). The Stromboli 2002 tsunamigenic submarine slide: Characteristics and possible failure mechanisms. *J. Geophys. Res.* 113, B10102. doi:10.1029/2007JB005172
- Civico, R., Ricci, T., Scarlato, P., Andronico, D., Cantarero, M., Carr, B. B., et al. (2021). Unoccupied aircraft systems (UASs) reveal the morphological changes at Stromboli volcano (Italy) before, between, and after the 3 July and 28 August 2019 paroxysmal eruptions. *Remote Sens. (Basel)*. 13, 2870. doi:10.3390/rs13152870
- Coppola, D., Piscopo, D., Laiolo, M., Cigolini, C., Delle Donne, D., Rippepe, M., et al. (2012). Radiative heat power at Stromboli volcano during 2000–2011: Twelve years of MODIS observations. *J. Volcanol. Geotherm. Res.* 215 (216), 48–60. doi:10.1016/j.jvolgeores.2011.12.001
- Corradino, C., Amato, E., Torrisi, F., Calvari, S., and Del Negro, C. (2021a). Classifying major explosions and paroxysms at Stromboli volcano (Italy) from space. *Remote Sens.* 13, 4080. doi:10.3390/rs13204080
- Corradino, C., Bilotta, G., Cappello, A., Fortuna, L., and Del Negro, C. (2021b). Combining radar and optical satellite imagery with machine learning to map lava flows at mount Etna and fogo island. *Energies* 14 (1), 197. doi:10.3390/en14010197
- Cutroneo, L., Ferretti, G., Barani, S., Scafidi, D., De Leo, F., Besio, G., et al. (2021). Near real-time monitoring of significant sea wave height through microseism recordings: Analysis of an exceptional sea storm event. *J. Mar. Sci. Eng.* 9 (3), 319. doi:10.3390/jmse9030319
- De Fino, M., La Volpe, L., Falsaperla, S., Frazzetta, G., Neri, G., Francalanci, L., et al. (1988). The Stromboli eruption of december 6, 1985–april 25, 1986: Volcanological, petrological and seismological data. *Rend Soc It Miner Petr* 43, 1021–1038.
- Di Lieto, B., Romano, P., Scarpa, R., and Linde, A. T. (2020). Strain signals before and during paroxysmal activity at Stromboli volcano, Italy. *Geophys. Res. Lett.* 47. doi:10.1029/2020GL088521
- Di Roberto, A., Bertagnini, A., Pompilio, M., and Bisson, M. (2014). Pyroclastic density currents at Stromboli volcano (aeolian islands, Italy): A case study of the 1930 eruption. *Bull. Volcanol.* 76, 827. doi:10.1007/s00445-014-0827-5
- Di Traglia, F., Battaglia, M., Nolesini, T., Lagomarsino, D., and Casagli, N. (2015). Shifts in the eruptive styles at Stromboli in 2010–2014 revealed by ground-based InSAR data. *Sci. Rep.* 5, 13569. doi:10.1038/srep13569
- Di Traglia, F., Calvari, S., D’Auria, L., Nolesini, T., Bonaccorso, A., Fornaciai, A., et al. (2018). The 2014 effusive eruption at Stromboli: New insights from *in situ* and remote-sensing measurements. *Remote Sens.* 10 (12), 2035. doi:10.3390/rs10122035
- Di Traglia, F., Cauchie, L., Casagli, N., and Saccorotti, G. (2014b). Decrypting geophysical signals at Stromboli Volcano (Italy): Integration of seismic and Ground-Based InSAR displacement data. *Geophys. Res. Lett.* 41 (8), 2753–2761. doi:10.1002/2014gl059824

- Di Traglia, F., De Luca, C., Manzo, M., Nolesini, T., Casagli, N., Lanari, R., et al. (2021). - Joint exploitation of space-borne and ground-based multitemporal InSAR measurements for volcano monitoring: The Stromboli volcano case study. *Remote Sens. Environ.* 260, 112441. doi:10.1016/j.rse.2021.112441
- Di Traglia, F., Fornaciari, A., Favalli, M., Nolesini, T., and Casagli, N. (2020). - catching geomorphological response to volcanic activity on steep slope volcanoes using multi- platform remote sensing. *Remote Sens. (Basel)*. 12 (3), 438. doi:10.3390/rs12030438
- Di Traglia, F., Nolesini, T., Intrieri, E., Mugnai, F., Leva, D., Rosi, M., et al. (2014a). Review of ten years of volcano deformations recorded by the ground-based InSAR monitoring system at Stromboli volcano: A tool to mitigate volcano flank dynamics and intense volcanic activity. *Earth-Science Rev.* 139, 317–335. doi:10.1016/j.earscirev.2014.09.011
- Finizola, A., Sortino, F., Lénat, J.-F., and Valenza, M. (2002). Fluid circulation at Stromboli volcano (Aeolian Islands, Italy) from self-potential and CO₂ surveys. *J. Volcanol. Geotherm. Res.* 116, 1–18. doi:10.1016/s0377-0273(01)00327-4
- Falsaperla, S., Maiolino, V., Spampinato, S., Jaquet, O., and Neri, M. (2008). Sliding episodes during the 2002 – 2003 Stromboli lava effusion: Insights from seismic, volcanic, and statistical data analysis. *Geochem. Geophys. Geosyst.* 9, Q04022. doi:10.1029/2007GC001859
- Falsaperla, S., Neri, M., Pecora, E., and Spampinato, S. (2006). Multidisciplinary study of flank instability phenomena at Stromboli volcano, Italy. *Geophys. Res. Lett.* 33, L09304. doi:10.1029/2006GL025940
- Fisher, J. B., Hook, S., Allen, R., Anderson, M. C., French, A. N., Hain, C., et al. (2015). “EcoStress: NASA’s next-generation mission to measure evapotranspiration from the international space station,” in *AGU fall meeting abstracts* (Washington, DC, USA: AGU).
- Francalanci, L., Tommasini, S., Conticelli, S., and Davies, G. R. (1999). Sr isotope evidence for short magma residence time for the 20th century activity at Stromboli volcano, Italy. *Earth Planet. Sci. Lett.* 167 (1–2), 61–69. doi:10.1016/S0012-821X(99)00013-8
- Francalanci, L., Lucchi, F., Keller, J., De Astis, G., and Tranne, C. A. (2013). *Eruptive, volcano-tectonic and magmatic history of the Stromboli volcano (north-eastern Aeolian archipelago)*, 37. London, Memoirs: Geological Society, 397–471. doi:10.1144/M37.13
- Ganci, G., Cappello, A., Zago, V., Bilotta, G., Héroult, A., Del Negro, C., et al. (2019). 3D Lava flow mapping of the 17–25 May 2016 Etna eruption using tri-stereo optical satellite data. *Ann. Geophys.* 62 (2). doi:10.4401/ag-7875
- Gabriel, A. K., Goldstein, R. M., and Zebker, H. A. (1989). Mapping small elevation changes over large areas: Differential radar interferometry. *J. Geophys. Res.* 94, 9183. doi:10.1029/JB094iB07p09183
- Gambino, S., Falzone, G., Ferro, A., and Laudani, G. (2014). Volcanic processes detected by tiltmeters: A review of experience on Sicilian volcanoes. *J. Volcanol. Geotherm. Res.* 271, 43–54. doi:10.1016/j.jvolgeores.2013.11.007
- Ganci, G., Bilotta, G., Calvari, S., Cappello, A., Del Negro, C., Héroult, A., et al. (2021). “Volcanic hazard monitoring using multi-source satellite imagery,” in 2021 IEEE International Geoscience and Remote Sensing Symposium IGARSS, Brussels, Belgium, 11–16 July 2021, 1903–1906. doi:10.1109/IGARSS47720.2021.9554557
- Ganci, G., Bilotta, G., Cappello, A., Héroult, A., and Del Negro, C. (2016). Hotsat: A multiplatform system for the thermal monitoring of volcanic activity using satellite data. *Geol. Soc. Lond. Spec. Publ.* 426, 207–221. doi:10.1144/SP426.21
- Ganci, G., Cappello, A., Bilotta, G., Héroult, A., Zago, V., Del Negro, C., et al. (2018). Mapping volcanic deposits of the 2011–2015 Etna eruptive events using satellite remote sensing. *Front. Earth Sci.* 6, 83. doi:10.3389/feart.2018.00083
- Ganci, G., Vicari, A., Fortuna, L., and Del Negro, C. (2011). The HOTSAT volcano monitoring system based on a combined use of SEVIRI and MODIS multispectral data. *Ann. Geophys.* 54, 5. doi:10.4401/ag-5338
- García-Aristizabal, A., Kumagai, H., Samaniego, P., Mothes, P., Yepes, H., Monzier, M., et al. (2007). Seismic, petrologic and geodetic analyses of the 1999 dome-forming eruption of Guagua Pichincha volcano, Ecuador. *J. Volcanol. Geotherm. Res.* 161 (4), 333–351. doi:10.1016/j.jvolgeores.2006.12.007
- Gillot, P. Y., and Keller, J. (1993). Radiochronological dating of Stromboli. *Acta Vulc* 3, 69–77.
- Giordano, G., and De Astis, G. (2021). The summer 2019 basaltic Vulcanian eruptions (paroxysms) of Stromboli. *Bull. Volcanol.* 83, 1. doi:10.1007/s00445-020-01423-2
- Giudicepietro, F., Esposito, A. M., Spina, L., Cannata, A., Morgavi, D., Layer, L., et al. (2021). Clustering of experimental seismo-acoustic events using self-organizing map (SOM). *Front. Earth Sci.* 8, 581742. doi:10.3389/feart.2020.581742
- Giudicepietro, F., Calvari, S., Alparone, S., Bianco, F., Bonaccorso, A., Bruno, V., et al. (2019). Integration of ground-based remote-sensing and *in situ* multidisciplinary monitoring data to analyze the eruptive activity of Stromboli volcano in 2017–2018. *Remote Sens. (Basel)*. 11, 1813. doi:10.3390/rs11151813
- Giudicepietro, F., Calvari, S., D’Auria, L., Di Traglia, F., Layer, L., Macedonio, G., et al. (2022). Changes in the eruptive style of Stromboli volcano before the 2019 paroxysmal phase discovered through SOM clustering of seismo-acoustic features compared with camera images and GBInSAR data. *Remote Sens.* 14, 1287. doi:10.3390/rs14051287
- Giudicepietro, F., Lopez, C., Macedonio, G., Alparone, S., Bianco, F., Calvari, S., et al. (2020). Geophysical precursors of the July–August 2019 paroxysmal eruptive phase and their implications for Stromboli volcano (Italy) monitoring. *Sci. Rep.* 10, 10296. doi:10.1038/s41598-020-67220-1
- Harris, A. J. L., and Stevenson, D. S. (1997). Magma budgets and steady-state activity of Vulcano and Stromboli. *Geophys. Res. Lett.* 24 (9), 1043–1046. doi:10.1029/97gl00861
- Harris, A., and Ripepe, M. (2007). Temperature and dynamics of degassing at Stromboli. *J. Geophys. Res.* 112, B03205. doi:10.1029/2006JB004393
- Herring, T. A., Floyd, M. A., King, R. W., and McClusky, S. C. (2015). “Globk: Global kalman filter VLBI and GPS analysis program,” in *Reference manual* (Cambridge: Massachusetts Institute of Technology).
- Herring, T. A., King, R. W., Floyd, M. A., and McClusky, S. C. (2018). “GPS analysis at MIT,” in *GAMIT reference manual* (Cambridge: Massachusetts Institute of Technology).
- Hornig-Kjarsgaard, I., Keller, J., Koberski, U., Stadlbauer, E., Francalanci, L., and Lenhart, R. (1993). Geology, stratigraphy and volcanological evolution of the island of Stromboli, Aeolian arc, Italy. *Acta Vulcanol.* 3, 21–68.
- Inguaggiato, S., Diliberto, I. S., Federico, C., Paonita, A., and Vita, F. (2018). Review of the evolution of geochemical monitoring, networks and methodologies applied to the volcanoes of the Aeolian Arc (Italy). *Earth-Science Rev.* 176, 241–276. doi:10.1016/j.earscirev.2017.09.006
- Inguaggiato, S., Vita, F., Cangemi, M., and Calderone, L. (2020). Changes in CO₂ soil degassing style as a possible precursor to volcanic activity: The 2019 case of Stromboli paroxysmal eruptions. *Appl. Sci. (Basel)*. 10, 4757. doi:10.3390/app10144757
- Inguaggiato, S., Vita, F., Cangemi, M., and Calderone, L. (2019). Increasing summit degassing at the Stromboli volcano and relationships with volcanic activity (2016–2018). *Geosciences* 9, 176. doi:10.3390/geosciences9040176
- Inguaggiato, S., Vita, F., Cangemi, M., Inguaggiato, C., and Calderone, L. (2021). The monitoring of CO₂ soil degassing as indicator of increasing volcanic activity: The paroxysmal activity at Stromboli volcano in 2019–2021. *Geosciences* 11, 169. doi:10.3390/geosciences11040169
- Inguaggiato, S., Vita, F., Cangemi, M., Mazot, A., Sollami, A., Calderone, L., et al. (2017). Stromboli volcanic activity variations inferred from observations of fluid geochemistry: 16 years of continuous monitoring of soil CO₂ fluxes (2000–2015). *Chem. Geol.* 469, 69–84. doi:10.1016/j.chemgeo.2017.01.030
- Inguaggiato, S., Vita, F., Rouwet, D., Bobrowski, N., Morici, S., Sollami, A., et al. (2011). Geochemical evidence of the renewal of volcanic activity inferred from CO₂ soil and SO₂ plume fluxes: The 2007 Stromboli eruption (Italy). *Bull. Volcanol.* 73 (4), 443–456. doi:10.1007/s00445-010-0442-z
- Karamanolakis, G., Hsu, D., and Gravano, L. (2019). *Weakly supervised attention networks for fine-grained opinion mining and public health*. Stroudsburg, PA, USA: Association for Computational Linguistics, 1–10.
- Landi, P., Francalanci, L., Pompilio, M., Rosi, M., Corsaro, R. A., Petrone, C. M., et al. (2006). The December 2002–July 2003 effusive event at Stromboli volcano, Italy: Insights into the shallow plumbing system by petrochemical studies. *J. Volcanol. Geotherm. Res.* 155, 263–284. doi:10.1016/j.jvolgeores.2006.03.032
- Lucchi, F., Francalanci, L., De Astis, G., Tranne, C. A., Braschi, E., Klaver, M., et al. (2019). Geological evidence for recurrent collapse-driven phreatomagmatic pyroclastic density currents in the Holocene activity of Stromboli volcano, Italy. *J. Volcanol. Geotherm. Res.* 385, 81–102. doi:10.1016/j.jvolgeores.2018.10.024
- Marani, M. P., Gamberi, F., Rosi, M., Bertagnini, A., and Di Roberto, A. (2009). Subaqueous density flow processes and deposits of an island volcano landslide (Stromboli Island, Italy). *Sedimentology* 56, 1488–1504. doi:10.1111/j.1365-3091.2008.01043.x
- Marotta, E., Calvari, S., Cristaldi, A., D’Auria, L., Di Vito, M. A., Moretti, R., et al. (2015). Reactivation of Stromboli’s summit craters at the end of the 2007 effusive

- eruption detected by thermal surveys and seismicity. *J. Geophys. Res. solid earth* 120, 7376–7395. doi:10.1002/2015JB012288
- Marsella, M., Baldi, P., Coltelli, M., and Fabris, M. (2012). The morphological evolution of the Sciara del Fuoco since 1868: Reconstructing the effusive activity at Stromboli volcano. *Bull. Volcanol.* 74, 231–248. doi:10.1007/s00445-011-0516-6
- Martini, M., Giudicepietro, F., D'Auria, L., Esposito, A. M., Caputo, T., Curciotti, R., et al. (2007). Seismological monitoring of the February 2007 effusive eruption of the Stromboli volcano. *Ann. Geophys.* 50, 775–788. doi:10.4401/ag-3056
- Mattia, M., Di Lieto, B., Ganci, G., Bruno, V., Romano, P., Ciancitto, F., et al. (2021). The 2019 eruptive activity at Stromboli volcano: A multidisciplinary approach to reveal hidden features of the “unexpected” 3 July paroxysm. *Remote Sens. (Basel)*. 13, 4064. doi:10.3390/rs13204064
- Merucci, L., Burton, M., Corradini, S., and Salerno, G. G. (2011). Reconstruction of SO₂ flux emission chronology from space-based measurements. *J. Volcanol. Geotherm. Res.* 206, 80–87. doi:10.1016/j.jvolgeores.2011.07.002
- Métrich, N., Bertagnini, A., Landi, P., Rosi, M., and Belhadj, O. (2005). Triggering mechanism at the origin of paroxysms at Stromboli (aeolian archipelago, Italy): The 5 April 2003 eruption. *Geophys. Res. Lett.* 32, L10305. doi:10.1029/2004GL022257
- Métrich, N., Bertagnini, A., and Pistolesi, M. (2021). Paroxysms at Stromboli volcano (Italy): Source, genesis and dynamics. *Front. Earth Sci.* 9, 593339. doi:10.3389/feart.2021.593339
- Neri, M., and Lanzafame, G. (2009). Structural features of the 2007 Stromboli eruption. *J. Volcanol. Geotherm. Res.* 182, 137–144. doi:10.1016/j.jvolgeores.2008.07.021
- Orazi, M., Martini, M., and Peluso, R. (2006). Data acquisition for volcano monitoring. *Eos Trans. AGU.* 87 (38), 385. doi:10.1029/2006eo380002
- Patané, D., Mattia, M., Di Grazia, G., Cannavò, F., Giampiccolo, E., Musumeci, C., et al. (2007). Insights into the dynamic processes of the 2007 Stromboli eruption and possible meteorological influences on the magmatic system. *Geophys. Res. Lett.* 34, L22309. doi:10.1029/2007GL031730
- Peccerillo, A., and Taylor, S. R. (1976). Geochemistry of eocene calc-alkaline volcanic rocks from the Kastamonu area, Northern Turkey. *Contr. Mineral. Pet.* 58 (1), 63–81. doi:10.1007/BF00384745
- Peltier, A., Villeneuve, N., Ferrazzini, V., Testud, S., Hassen Ali, T., Boissier, P., et al. (2018). Changes in the long-term geophysical eruptive precursors at Piton de la Fournaise: Implications for the response management. *Front. Earth Sci.* 6, 104. doi:10.3389/feart.2018.00104
- Pichavant, M., Di Carlo, I., Pompilio, M., and Le Gall, N. (2022). Timescales and mechanisms of paroxysm initiation at Stromboli volcano, Aeolian Islands, Italy. *Italy. Bull. Volcanol.* 84, 36. doi:10.1007/s00445-022-01545-9
- Pioli, L., Rosi, M., Calvari, S., Spampinato, L., Renzulli, A., and Di Roberto, A. (2008). “The eruptive activity of 28 and 29 December 2002,” in *The Stromboli volcano: An integrated study of the 2002–2003 eruption*. Editors S. Calvari, S. Inguaggiato, G. Puglisi, M. Ripepe, and M. Rosi, 182, 105–116. Washington, D.C.: American Geophysical Union Monograph Series. doi:10.1029/182GM10
- Plank, S., Marchese, F., Filizzola, C., Pergola, N., Neri, M., Nolde, M., et al. (2019). The July/August 2019 Lava Flows at the Sciara del Fuoco, Stromboli—Analysis from Multi-Sensor Infrared Satellite Imagery. *Remote Sens. (Basel)*. 11, 2879. doi:10.3390/rs11232879
- Platt, A., and Stutz, U. (2008). *Differential optical absorption spectroscopy - principles and applications*. Heidelberg: Springer. doi:10.1007/978-3-540-75776-4
- Ripepe, M., Delle Donne, D., Lacanna, G., Marchetti, E., and Ulivieri, G. (2009). The onset of the 2007 Stromboli effusive eruption recorded by an integrated geophysical network. *J. Volcanol. Geotherm. Res.* 182, 131–136. doi:10.1016/j.jvolgeores.2009.02.011
- Rittmann, A. (1931). Der ausbruch des Stromboli am 11 September 1930. *Z. für Vulkanol.* 14, 47–77.
- Roeloffs, E. A., and Linde, A. T. (2007). “Borehole observations of continuous strain and fluid pressure,” in *Volcano deformation* (Berlin, Heidelberg: Springer). Springer Praxis Books. doi:10.1007/978-3-540-49302-0_9
- Romagnoli, C., Casalbore, D., Bortoluzzi, G., Bosman, A., Chiocci, F. L., D’Orlando, F., et al. (2013). Chapter 4 bathy-morphological setting of the aeolian islands. *Geol. Soc. Lond. Memoirs* 37, 27–36. doi:10.1144/m37.4
- Romagnoli, C., Kokelaar, P., Rossi, P. L., and Sodi, A. (1993). The submarine extension of Sciara del Fuoco feature (Stromboli isl.): Morphologic characterization. *Acta Vulcanol.* 3, 91–98.
- Roy, D. P., Wulder, M. A., Loveland, T. R., Woodcock, C. E., Allen, R. G., Anderson, M. C., et al. (2014). Landsat-8: Science and product vision for terrestrial global change research. *Remote Sens. Environ.* 145, 154–172. doi:10.1016/j.rse.2014.02.001
- Rudolf, H., Leva, D., Tarchi, D., and Sieber, A. J. (1999). “A mobile and versatile SAR system,” in IEEE 1999 International Geoscience and Remote Sensing Symposium, Hamburg, Germany, 28 June 1999 - 02 July 1999, 592–594. IGARSS’99 (Cat. No. 99CH36293).
- Sacks, S., Suyehiro, S., Evertson, D. W., and Yamagishi, Y. (1971). Sacks-Evertson strainmeter, its installation in Japan and some preliminary results concerning strain steps. *Pap. Mater. Geophys.* 22, 195–208. doi:10.2467/mripapers1950.22.3-4_195
- Salerno, G. G., Burton, M., Di Grazia, G., Caltabiano, T., and Oppenheimer, C. (2018). Coupling between magmatic degassing and volcanic tremor in basaltic volcanism. *Front. Earth Sci.* 6, 157. doi:10.3389/feart.2018.00157
- Salerno, G. G., Burton, M. R., Oppenheimer, C., Caltabiano, T., Randazzo, D., Bruno, N., et al. (2009a). Three-years of SO₂ flux measurements of Mt. Etna using an automated UV scanner array: Comparison with conventional traverses and uncertainties in flux retrieval. *J. Volcanol. Geotherm. Res.* 183, 76–83. doi:10.1016/j.jvolgeores.2009.02.013
- Salerno, G. G., Burton, M. R., Oppenheimer, C., Caltabiano, T., Tsanev, V., Bruno, N., et al. (2009b). Novel retrieval of volcanic SO₂ abundance from ultraviolet spectra. *J. Volcanol. Geotherm. Res.* 181, 141–153. doi:10.1016/j.jvolgeores.2009.01.009
- Salvatici, T., Di Roberto, A., Di Traglia, F., Bisson, M., Morelli, S., Fidolini, F., et al. (2016). From hot rocks to glowing avalanches: Numerical modelling of gravity-induced pyroclastic density currents and hazard maps at the Stromboli volcano (Italy). *Geomorphology* 273, 93–106. doi:10.1016/J.GEOMORPH.2016.08.011
- Schaefer, L. N., Di Traglia, F., Chaussard, E., Lu, Z., Nolesini, T., Casagli, N., et al. (2019). Monitoring volcano slope instability with synthetic aperture radar: A review and new data from pacaya (Guatemala) and Stromboli (Italy) volcanoes. *Earth-Science Rev.* 192, 236–257. doi:10.1016/j.earscirev.2019.03.009
- Schmid, M., Kueppers, U., Civico, R., Ricci, T., Taddeucci, J., Dingwell, D. B., et al. (2021). Characterising vent and crater shape changes at Stromboli: Implications for risk areas. *Volcanica* 4 (1), 87–105. doi:10.30909/vol.04.01.87105
- Silvestri, M., Marotta, E., Buongiorno, M. F., Avvisati, G., Belviso, P., Bellucci Sessa, E., et al. (2020a). Monitoring of surface temperature on parco delle biancane (Italian geothermal area) using optical satellite data, UAV and field campaigns. *Remote Sens. (Basel)*. 12 (12), 2018. doi:10.3390/rs12122018
- Silvestri, M., Romaniello, V., Hook, S., Musacchio, M., Teggi, S., Buongiorno, M. F., et al. (2020b). First comparisons of surface temperature estimations between ECOSTRESS, ASTER and Landsat 8 over Italian volcanic and geothermal areas. *Remote Sens. (Basel)*. 12 (1), 184. doi:10.3390/rs12010184
- Solana, M. C., Calvari, S., Kilburn, C. R. J., Gutierrez, H., Chester, D., and Duncan, A. (2017). “Supporting the development of procedures for communications during volcanic emergencies: Lessons learnt from the canary islands (Spain) and Etna and Stromboli (Italy),” in *Advances in Volcanology, observing the volcano world, volcano crisis communication*. Editors C. J. Fearnley, D. K. Bird, K. Haynes, W. J. McGuire, and G. Jolly (Switzerland AG: Springer Open), 289–305. ISBN 978-3-319-44095-8. doi:10.1007/11157_2016_48
- Spampinato, L., Calvari, S., Oppenheimer, C., and Lodato, L. (2008). Shallow magma transport for the 2002–3 Mt. Etna eruption inferred from thermal infrared surveys. *J. Volcanol. Geotherm. Res.* 177, 301–312. doi:10.1016/j.jvolgeores.2008.05.013
- Tibaldi, A. (2001). Multiple sector collapses at Stromboli volcano, Italy: How they work. *Bull. Volcanol.* 63, 112–125. doi:10.1007/s004450100129
- Tinti, S., Manucci, A., Pagnoni, G., Armigliato, A., and Zaniboni, F. (2005). The 30 December 2002 landslide-induced tsunamis in Stromboli: Sequence of the events reconstructed from the eyewitness accounts. *Nat. Hazards Earth Syst. Sci.* 5, 763–775. doi:10.5194/nhess-5-763-2005
- Tioukov, V., Giudicepietro, F., Macedonio, G., Calvari, S., Di Traglia, F., Fornaciari, A., et al. (2022). “Structure of the shallow supply system at Stromboli volcano, Italy, through integration of muography, digital elevation models, seismicity, and ground deformation data,” in *Muography: Exploring earth’s subsurface with elementary particles*. Editors L. Olah, H. K. M. Tanaka, and D. Varga (Hoboken, NJ: Wiley), 75–91. American Geophysical Union, Geophysical Monograph 270. doi:10.1002/9781119722748
- Tommasi, P., Baldi, P., Chiocci, F. L., Coltelli, M., Marsella, M., Pompilio, M., et al. (2005). “The landslide sequence induced by the 2002 eruption at Stromboli volcano,” in *Landslide - risk analysis and sustainable disaster management*. Editors K. Sassa, H. Fukuoka, F. W. Wang, and G. Wang (Springer-Verlag), 251–258. ISBN: 3-540-28664-0.
- Walker, G. P. L. (1971). Grain-size characteristics of pyroclastic deposits. *J. Geol.* 79, 696–714. doi:10.1086/627699

- Wan, Z. (2014). New refinements and validation of the collection-6 MODIS land-surface temperature/emissivity product. *Remote Sens. Environ.* 140, 36–45. doi:10.1016/j.rse.2013.08.027
- Washington, H. S. (1917). Persistence of vents at Stromboli and its bearing on volcanic mechanism. *Geol. Soc. Am. Bull.* 28, 249–278. doi:10.1130/gsab-28-249
- Wu, L., Zheng, S., De Santis, A., Qin, K., Di Mauro, R., Liu, S., et al. (2016). Geosphere coupling and hydrothermal anomalies before the 2009 M_w 6.3 L'Aquila earthquake in Italy. *Nat. Hazards Earth Syst. Sci.* 16, 1859–1880. doi:10.5194/nhess-16-1859-2016
- Yamaguchi, Y., Kahle, A. B., Tsu, H., Kawakami, T., and Pniel, M. (1998). Overview of advanced spaceborne thermal emission and reflection radiometer (ASTER). *IEEE Trans. Geosci. Remote Sens.* 36 (4), 1062–1071. doi:10.1109/36.700991
- Zago, V., Bilotta, G., Cappello, A., Dalrymple, R. A., Fortuna, L., Ganci, G., et al. (2017). Simulating complex fluids with smoothed particle hydrodynamics. *Ann. Geophys.* 60 (6). doi:10.4401/ag-7362
- Zago, V., Bilotta, G., Cappello, A., Dalrymple, R. A., Fortuna, L., Ganci, G., et al. (2019). Preliminary validation of lava benchmark tests on the GPUSPH particle engine. *Ann. Geophys.* 62 (2), VO224. doi:10.4401/ag-7870
- Zanon, V., Neri, M., and Pecora, E. (2009). Interpretation of data from the monitoring thermal camera of Stromboli volcano (Aeolian Islands, Italy). *Geol. Mag.* 146 (4), 591–601. doi:10.1017/s0016756809005937
- Zhou, S., Tordesillas, A., Intrieri, E., Di Traglia, F., Qian, G., Catani, F., et al. (2022). Pinpointing early signs of impending slope failures from space. *JGR. Solid Earth* 127, e2021JB022957. doi:10.1029/2021JB022957